

Heat Transfer Analysis of MHD Nanofluids in a Rotating Channel with Heat Source and Radiation



By
Sofia Sarwar


Supervised by
Dr. Moniba Shams

School of Natural Sciences
Department of Mathematics
National University of Sciences and Technology
H-12, Islamabad, Pakistan
2021

© Sofia Sarwar, 2021

National University of Sciences & Technology**MS THESIS WORK**

We hereby recommend that the dissertation prepared under our supervision by: **Sofia Sarwar**, Regn No. **00000321420** Titled: "**Heat Transfer Analysis of MHD Nanouids in a Rotating Channel with Heat Source and Radiation**" accepted in partial fulfillment of the requirements for the award of **MS** degree.

Examination Committee Members1. Name: DR. M. ASIF FAROOQSignature: 2. Name: DR. ASIM AZIZSignature: External Examiner: DR. RIZWAN UL HAQSignature:  18/01/2022Supervisor's Name: DR. MONIBA SHAMSSignature:  18/01/2022


Head of Department

18/01/2022
Date

COUNTERSIGNEDDate: 19.01.2022


Dean/Principal

Dedicated to my parents and siblings.

Acknowledgment

First of all i would like to thank **Allah (SWT)** for His countless blessings and the strength and knowledge. He has blessed me to carry out this research work.

I would like to express my sincere gratitude to my supervisor **Dr. Moniba Shams** for her support and guidance throughout this work. Her motivation and kind attitude helped me stay focused.

My sincere gratitude to GEC members **Dr. Muhammad Asif Farooq (SNS)** and **Dr. Asim Aziz (EME)** for their valuable guidance which enable me to complete this research.

I thank my parents for their support, prayers and love, that lead me to be the person who I am today. I could not be able to stand firm in my life without them. They are the reason behind my success. I also wanted to thank my siblings for cheering me up and for their moral support.

I would like to extend my gratitude towards my friends **Muhammad Faraz, Humna Arshad** and **Masoom Zahra** for their continuous support. They were always there whenever I needed them. I am thankful to everyone who helped me throughout my MS mathematics program.

Sofia Sarwar

Abstract

In this thesis work, effect of heat transfer on single and multiple walled carbon nanotubes between two rotating plates, in the presence of transverse applied magnetic field, linear thermal radiation and the constant heat source is observed. The governing partial differential equations (PDEs) are transformed into ordinary differential equations (ODEs) by using a set of similarity transformations. Thereafter using MATLAB (*bvp4c*), the numerical solutions are obtained. Numerical computations are carried out for water based single walled and multiple walled carbon nanotubes respectively. The impact of governing physical parameters including nanoparticle volume fraction (ϕ), suction/injection (S), reynolds number (A_1), rotation (A_2), magnetic parameter (M), thermal radiation (Nr) and heat generation or absorption parameter (Q) on velocity and temperature profiles are studied. The skin friction coefficient and local Nusselt number are also analyzed.

Contents

1	Introduction	1
2	Basic Definitions	4
2.1	Fluid mechanics	4
2.2	Specific heat capacity	4
2.3	Steady and unsteady flow	5
2.4	Laminar flow	5
2.5	Turbulent flow	5
2.6	Viscosity	6
2.6.1	Dynamic viscosity	6
2.6.2	Kinematic viscosity	6
2.7	Thermal conductivity	6
2.8	Thermal diffusivity	7
2.9	Heat Flux	7
2.10	Nanofluids	8
2.11	Carbon nanotubes	8
2.12	Centripetal force	8

2.13	Coriolis force	9
2.14	Free and Forced convection	9
2.15	Dimensionless parameters	9
2.15.1	Prandtl number	9
2.15.2	Nusselt number	10
2.15.3	Reynolds number	10
2.15.4	Skin friction coefficient	11
2.16	Continuity equation	11
2.17	Momentum equation	12
2.18	Energy equation	13
3	Water driven flow of carbon nanotubes in a rotating channel	14
3.1	Problem geometry	14
3.2	Results and Discussion	21
3.2.1	Velocity and Temperature	21
3.2.2	Local Nusselt number and the skin friction coefficient	26
4	Thermal radiation and heat source effect on MHD flow of carbon nanotubes in a rotating channel	35
4.1	Mathematical formulation	36
4.2	Numerical method	41
4.3	Results and discussion	42
4.3.1	Velocity and temperature	42
4.3.2	Skin friction coefficient (C_f^*) and local Nusselt number (Nu_x^*)	48
5	Conclusions	53

List of Figures

3.1	Schematic figure of the problem [19]	15
3.2	Velocity variation in (a-b) and temperature in (c) with respect to η for diverse choices of ϕ	22
3.3	Velocity variation in (a-b) and temperature in (c) with respect to η for diverse choices of S	23
3.4	Velocity variation in (a-b) and temperature in (c) with respect to η for diverse choices of A_1	24
3.5	Velocity variation in (a-b) and temperature in (c) with respect to η for diverse choices of A_2	25
3.6	Fluctuation of the skin friction coefficient (Eq. (3.29)) at $\eta = 0$ for SW_{CNT} and MW_{CNT} against different values of S , A_1 and A_2	28
3.7	Fluctuation of the skin friction coefficient (Eq. (3.29)) at $\eta = 1$ for SW_{CNT} and MW_{CNT} against different values of S , A_1 and A_2	30
3.8	Fluctuation of local Nusselt number (Eq. (3.30)) at $\eta = 0$ for SW_{CNT} and MW_{CNT} against different choices of S , A_1 and A_2	33
3.9	Fluctuation of local Nusselt number (Eq. 3.30) at $\eta = 1$ for SW_{CNT} and MW_{CNT} against different choices of S , A_1 and A_2	34

4.1	Flow field geometry	36
4.2	Velocity variation in (a-b) and temperature in (c) with respect to η for diverse choices of ϕ with $Bi = 10$	43
4.3	Velocity variation in (a-b) and temperature in (c) with respect to η for diverse choices of S with $Bi = 10$	44
4.4	Velocity variation in (a-b) and temperature in (c) with respect to η for diverse choices of A_1 with $Bi = 10$	45
4.5	Velocity variation in (a-b) and temperature in (c) with respect to η for diverse choices of A_2 with $Bi = 10$	46
4.6	Velocity variation with respect to η for diverse choices of M	47
4.7	Temperature variation for diverse choices of Nr and Q with $Bi = 10$	47

Chapter 1

Introduction

Nanofluids are made up by including solid nanoparticles that are evenly and consistently distributed in the base fluid. There are many applications of nanofluids in the industrial setups, for example, significant amount of unwanted heat is generated in industrial devices and nanofluids are used as a coolant as they increase the thermal conductivity of fluid. They are also used in various solar systems including PV/thermal (PV/T), collectors and water heating technologies. Masuda et al. [1] showed that with the addition of ultra-fine sized particles (nanoparticles), the thermal conductivity of ordinary fluid can be increased. Choi and Eastman [2] was the first one who gave the idea of nanofluids and proposed its use in energy production, electronics, textiles, and paper manufacturing. Xie et al. [3] studied the enhanced thermal properties of nanofluids containing carbon nanotubes (C_{NT}).

Heat transfer induced by fluid flow is a major research field in fluid mechanics. Therefore, researchers have paid attention to heat transfer mechanism. Recent studies [4-5] shows that in the presence of magnetic field, thermal conductivity in nanofluids increases. Chamkha and Aly [6] described the effect of heat generation and absorption

on MHD flow of nanofluids. Haq et. al [7-8] investigated the effect of volume fraction of C_{NT} on heat transfer over a stretching sheet.

Radiation increases the temperature of the fluid which in turn increases the thermal conductivity of the fluid. Motsumi and Makinde [9] and Shehzad et. al [10] studied the thermal radiation effect on nanofluids. It was observed that both velocity and temperature of the nanofluid increases with the increase in radiation parameter. Many researchers [11-14] examined the effect of thermal radiation on MHD flow of nanofluids. In turbomachinery, rotating flows are used in variety of ways. [15-17] presented the study of flow of nanotubes in a rotating frame of reference. Sheikholeslami and Ganji [18] studied the MHD flow of nanofluid and heat transfer with the effect of radiation. Hussain et.al [19] investigated the rotation effect on fluid flow of C_{NT} . It was observed that in comparison with MW_{CNT} , SW_{CNT} have reduced drag and high rate of heat transfer. In a recent study, Jawed et. al [20] described the effect of radiation on the rotating flow of C_{NT} .

The goal of the present research is to analyze heat transfer and flow of C_{NT} in the presence of applied uniform magnetic field, thermal radiation and the constant heat source, between two rotating plates. Suction / injection (S), reynolds number A_1 , rotation parameter A_2 , nanoparticle volume fraction (ϕ), magnetic parameter (M), rate of heat generation or absorption coefficient (Q) and thermal radiation (Nr), influence on local nusselt number and the skin friction coefficient are discussed and analyzed. The MATLAB package *bvp4c* is used to find numerical similarity solutions of reduced nonlinear ordinary differential equations.

The overview of the thesis is as follows:

The second chapter includes basic definitions of fluid mechanics. Definitions of some dimensionless parameters, thermophysical properties of C_{NT} and equations used fur-

ther in the thesis.

In chapter 3, detailed review of Hussain et.al [19] is presented. Here the heat transfer and the rotation effect of C_{NT} is analyzed. Using similarity transformations, set of PDEs is converted into a set of ODEs with given boundary conditions. Graphical and tabular results of velocity and temperature profiles along with the local Nusselt number and skin friction coefficient for various parameters are discussed and illustrated graphically.

Chapter 4 extends the problem presented in chapter 3. Effect of magnetic field, thermal radiation and heat source on C_{NT} (water as basefluid) in a rotating channel is observed. Graphical and tabular results are obtained for different parameters including the local Nusselt number and the Skin friction coefficient.

Chapter 5 includes the concluding remarks of this dissertation.

Chapter 2

Basic Definitions

In this chapter we will define some basic concepts of fluid mechanics. Some definitions are taken from the book of White [21].

2.1 Fluid mechanics

Fluid mechanics is the branch of applied mathematics which deals the behavior of fluids at dynamic and static situations. It handles relationship between force, motion and statistical condition in a continuous material.

2.2 Specific heat capacity

The amount of heat required to raise the temperature of a substance of one kilogram mass by one degree with constant pressure is called the specific heat. It is denoted by C_p and given by

$$C_p = \frac{q}{\nabla T}, \quad (2.1)$$

where q is the supplied heat and ∇T is the difference in temperature. Since heat is added into the system, therefore, specific heat can't be negative.

2.3 Steady and unsteady flow

A steady flow is one in which physical quantities do not change with time. Mathematically,

$$\frac{\partial y}{\partial t} = 0, \quad (2.2)$$

where y is any physical quantity (density, velocity, pressure etc) of fluid and t represent the time. If these physical quantities change with time then it is an unsteady flow.

2.4 Laminar flow

When the fluid particles moves regularly and evenly then the flow is known as laminar flow. This flow is linked with Reynolds number, when viscous force is dominant and Reynolds number is low then the fluid particles do not cut through each other.

2.5 Turbulent flow

When the fluid particles move irregularly in all directions and they cut through each other then the flow is called turbulent flow. When inertial forces dominate and Reynolds number is high then it causes turbulent flow.

2.6 Viscosity

The viscosity of a fluid is a measurement of its resistance to flow.

There are two types of viscosities. One is dynamic viscosity and the other is kinematic viscosity.

2.6.1 Dynamic viscosity

Dynamic viscosity is a measurement of fluid's internal resistance to flow when subjected to external forces. It is denoted by μ . Higher viscosity indicates that fluid is thick and lower viscosity means fluid is thin.

2.6.2 Kinematic viscosity

Kinematic viscosity is the ratio of dynamic viscosity (μ) to the density (ρ). It is a measure of fluid's resistance to shear flow under the weight of gravity. It tells us how fast a fluid is moving when certain amount of force is applied.

$$\nu = \frac{\mu}{\rho}. \quad (2.3)$$

2.7 Thermal conductivity

The ability of a given material to transfer heat per unit time is known as the thermal conductivity (κ),

$$\kappa = \frac{Qd}{A\nabla T}, \quad (2.4)$$

where Q is the total transferred heat, d is the distance between two isothermal planes in which heat is transferred, A is the area of the surface and ∇T is the temperature differ-

ence. Higher value of thermal conductivity means the rate at which heat is transferred through the material is high.

2.8 Thermal diffusivity

The ratio of thermal conductivity to the specific heat capacity and density where pressure is kept constant is defined as thermal diffusivity (α). Mathematically,

$$\alpha = \frac{\kappa}{\rho C_p}. \quad (2.5)$$

It is clear that larger value of thermal diffusivity means fast distribution of heat into the material and if its value is small, then it shows that large amount of heat is absorbed by the material. Lower value of C_p means less energy is required to raise the temperature of one unit volume by one degree kelvin.

2.9 Heat Flux

Heat flux is defined as the amount of heat transferred per unit area per unit time, to/from a surface. The rate of thermal energy that passes through a surface is called heat flux (ϕ_q). It always flows from the higher temperature to lower temperature.

$$\phi_q = -\kappa \nabla \vec{T}. \quad (2.6)$$

2.10 Nanofluids

Fluids containing nano-sized suspended solid particles are known as nanofluids. They are two phased systems, one is solid phase and other is liquid. In comparison with other base fluids like water and oil, nanofluids have enhanced thermophysical properties like thermal conductivity, thermal diffusivity, viscosity and convective heat transfer coefficients. Nanofluids are efficient heat transfer fluids and are used in many thermal energy systems to improve the systems efficiency.

2.11 Carbon nanotubes

Carbon nanotubes are hexagonally shaped arrangements of carbon atoms (graphene), rolled into tubes. They were discovered by Iijima [22]. Carbon nanotubes have high thermal conductivity, mechanical strength and corrosion resistance. There are single wall carbon nanotubes (SW_{CNT}) that can have diameter less than 1 nm and there are also multiple wall carbon nanotubes (MW_{CNT}) that can have diameter upto 100 nm.

2.12 Centripetal force

A net force that act on an object to move it in a circular path is called a centripetal force and is directed towards the center of curvature.

In Newton's second law of motion ($F = ma$), m is the mass of the object and a is the acceleration. When circular motion is uniform then, $a = a_c$ (centripetal acceleration).

The expression for the centripetal force F_c is given by

$$F_c = \frac{mv^2}{r}, \quad (2.7)$$

where m is the mass of the object, v is the speed or velocity of the object and r is the radius.

2.13 Coriolis force

An apparent deflective force that acts on moving objects as a result of rotation of earth is known as coriolis force.

$$F = 2m(\boldsymbol{\Omega} \times \mathbf{V}), \quad (2.8)$$

where $\boldsymbol{\Omega}$ is angular velocity and \mathbf{V} is tangential velocity.

2.14 Free and Forced convection

When motion of fluid occurs due to natural means then it is free (natural) convection.

When fluid is obligated to move due to some external forces then it is forced convection.

2.15 Dimensionless parameters

Throughout this thesis various parameters will appear. The pertinent parameters are collected with brief detail in this section.

2.15.1 Prandtl number

Prandtl number is the ratio of kinematic viscosity to thermal diffusivity. It is dimensionless and usually used in heat transfer as well as natural and forced convection

problems in fluid mechanics. Mathematically,

$$Pr = \frac{\nu}{\alpha}, \quad (2.9)$$

substitution of Eq. (2.3) and Eq. (2.5) in Eq. (2.9) gives

$$Pr = \frac{\mu C_p}{\kappa}. \quad (2.10)$$

Small values of Prandtl number means fluid has high thermal conductivity and is therefore a good choice for heat conducting liquids. Prandtl number can't be zero because both kinematic viscosity and thermal diffusivity are physical parameters of fluid and have positive values.

2.15.2 Nusselt number

Nusselt number is a dimensionless parameter defined as the ratio of convective to conductive heat transfer coefficient. Mathematically,

$$Nu = \frac{hL}{\kappa}, \quad (2.11)$$

where h is heat transfer coefficient and L is characteristic length.

2.15.3 Reynolds number

Reynolds number determines the ratio of inertial and viscous forces. It is denoted by Re and plays a very significant role in anticipating the behavior of the fluid. High Reynolds number means fluid's behavior is turbulent due to dominant inertial forces

and low Reynolds number means viscous forces are dominant. Mathematically,

$$Re = \frac{vL}{\nu}. \quad (2.12)$$

2.15.4 Skin friction coefficient

The friction which is caused when fluid experiences a resistance against direction of flow on any solid surface is known as the skin friction. The skin friction coefficient C_f is defined as

$$C_f = \frac{\tau_w}{\rho \mathbf{U}_v^2}, \quad (2.13)$$

where U_v is the free stream velocity, τ_w represents the local wall shear stress and is expressed as

$$\tau_w = \mu_{nf} \frac{\partial u}{\partial y}.$$

2.16 Continuity equation

The continuity equation (conservation of mass) is given as

$$\frac{\partial \rho}{\partial t} + \vec{\nabla} \cdot (\rho \vec{v}) = 0, \quad (2.14)$$

when the flow is incompressible, that is

$$\frac{\partial \rho}{\partial t} = 0, \quad (2.15)$$

the Eq. (2.14) becomes

$$\rho \vec{\nabla} \cdot \vec{v} = 0. \quad (2.16)$$

as density ρ is scalar quantity then Eq. (2.16) becomes

$$\vec{\nabla} \vec{v} = 0. \quad (2.17)$$

2.17 Momentum equation

According to Newton's second law of motion, momentum of a system remains constant until an external force is applied. It can be expressed as

$$\rho \frac{d\vec{V}}{dt} = \nabla \cdot \tau + \rho \cdot \vec{g}, \quad (2.18)$$

where $\nabla \cdot \tau$ represents the surface force and $\rho \cdot \vec{g}$ represents the body force in the system.

$$\nabla \cdot \tau = -\nabla P + \mu \nabla^2 \vec{V} \quad (2.19)$$

substituting Eq. (2.19) in Eq. (2.18) gives

$$\rho \frac{d\vec{V}}{dt} = -\nabla P + \mu \nabla^2 \vec{V} + \rho \vec{g}. \quad (2.20)$$

It is also known as Navier-Stokes equation. If $\vec{V} = V(\mathbf{U}_1(x, y, z, t), \mathbf{U}_2(x, y, z, t), \mathbf{U}_3(x, y, z, t))$, then Eq. (2.20) can be written in component form as
x-component

$$\rho \left(\frac{\partial \mathbf{U}_1}{\partial t} + \mathbf{U}_1 \frac{\partial \mathbf{U}_1}{\partial x} + \mathbf{U}_2 \frac{\partial \mathbf{U}_1}{\partial y} + \mathbf{U}_3 \frac{\partial \mathbf{U}_1}{\partial z} \right) = -\frac{\partial p}{\partial x} + \mu \left(\frac{\partial^2 \mathbf{U}_1}{\partial x^2} + \frac{\partial^2 \mathbf{U}_1}{\partial y^2} + \frac{\partial^2 \mathbf{U}_1}{\partial z^2} \right) + \rho g_x, \quad (2.21)$$

y-component

$$\rho\left(\frac{\partial \mathbf{U}_2}{\partial t} + \mathbf{U}_1 \frac{\partial \mathbf{U}_2}{\partial x} + \mathbf{U}_2 \frac{\partial \mathbf{U}_2}{\partial y} + \mathbf{U}_3 \frac{\partial \mathbf{U}_2}{\partial z}\right) = -\frac{\partial p}{\partial y} + \mu\left(\frac{\partial^2 \mathbf{U}_2}{\partial x^2} + \frac{\partial^2 \mathbf{U}_2}{\partial y^2} + \frac{\partial^2 \mathbf{U}_2}{\partial z^2}\right) + \rho g_y, \quad (2.22)$$

z-component

$$\rho\left(\frac{\partial \mathbf{U}_3}{\partial t} + \mathbf{U}_1 \frac{\partial \mathbf{U}_3}{\partial x} + \mathbf{U}_2 \frac{\partial \mathbf{U}_3}{\partial y} + \mathbf{U}_3 \frac{\partial \mathbf{U}_3}{\partial z}\right) = -\frac{\partial p}{\partial z} + \mu\left(\frac{\partial^2 \mathbf{U}_3}{\partial x^2} + \frac{\partial^2 \mathbf{U}_3}{\partial y^2} + \frac{\partial^2 \mathbf{U}_3}{\partial z^2}\right) + \rho g_z, \quad (2.23)$$

2.18 Energy equation

Law of conservation of energy can be written as

$$\rho C_p (\mathbf{V} \cdot \nabla) T = -\nabla \cdot \mathbf{q}, \quad (2.24)$$

by using Fourier's law of heat transfer

$$\mathbf{q} = -\kappa \nabla T, \quad (2.25)$$

substituting Eq. (2.25) in Eq. (2.24) we get

$$\rho C_p (\mathbf{V} \cdot \nabla) T = \kappa (\nabla^2 T). \quad (2.26)$$

Chapter 3

Water driven flow of carbon nanotubes in a rotating channel

This chapter describes the review of an article by Hussain et.al [19] which describes the heat transfer and flow of C_{NT} with water as base fluid in a rotating channel. By using a set of similarity transformations, the governing partial differential equations are converted into non-linear ordinary differential equations and solved numerically by using `bvp4c`, a built-in solver of MATLAB. The fluctuations of velocity profile, temperature profile, local Nusselt number and the skin friction are presented graphically for various values of governing parameters.

3.1 Problem geometry

In a rotating frame of reference, consider a physical model that consists of two infinite plates, the plate on the top is permeable and the plate at the bottom is moving with variable velocity $\mathbf{U}_v=mx$ ($m > 0$). Let the temperature at the upper wall is T_0 and

the temperature at lower wall is T_a i.e $T_a > T_0$. Assume a steady, two dimensional, incompressible flow of C_{NT} within base fluid (water) between the infinite plates. The simplified geometrical representation of the problem is depicted

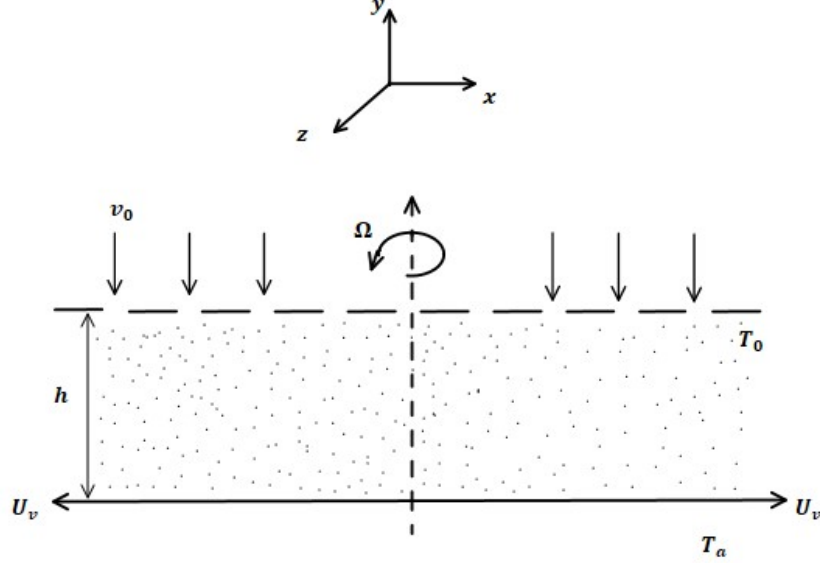


Figure 3.1: Schematic figure of the problem [19]

For the given flow, the momentum equation is given as

$$\rho_{nf} \left(\frac{d\mathbf{V}}{dt} + 2\boldsymbol{\Omega} \times \mathbf{V} + \boldsymbol{\Omega} \times (\boldsymbol{\Omega} \times \mathbf{r}) \right) = \text{div}\mathbf{T}, \quad (3.1)$$

where $2(\boldsymbol{\Omega} \times \mathbf{V})$ is the coriolis force and $\boldsymbol{\Omega} \times (\boldsymbol{\Omega} \times \mathbf{r})$ is the centripetal force. In rotating flow, both forces are produced due to the variable velocity of the lower wall. Velocity field is denoted as $\mathbf{V}[\mathbf{U}_1(x, y), \mathbf{U}_2(x, y), \mathbf{U}_3(x, y)]$ where \mathbf{U}_1 , \mathbf{U}_2 and \mathbf{U}_3 are the velocity components along x , y and z directions respectively. Coriolis and centripetal forces are perpendicular to \mathbf{V} and $\boldsymbol{\Omega}$, and are directed towards y -axis (axis of rotation).

The continuity equation in cartesian coordinates system is given as

$$\frac{\partial \rho}{\partial t} + \rho \vec{\nabla} \cdot \vec{v} = 0, \quad (3.2)$$

As the given flow is steady, incompressible and two dimensional then Eq. (3.2) will become

$$\frac{\partial \mathbf{U}_1}{\partial x} + \frac{\partial \mathbf{U}_2}{\partial y} = 0. \quad (3.3)$$

The coriolis force $2(\boldsymbol{\Omega} \times \mathbf{V})$ for $\mathbf{V} = (\mathbf{U}_1, \mathbf{U}_2, \mathbf{U}_3)$ and angular velocity $\boldsymbol{\Omega} = (0, \Omega, 0)$ can be written as

$$2(\boldsymbol{\Omega} \times \mathbf{V}) = 2 \begin{vmatrix} i & j & k \\ 0 & \Omega & 0 \\ \mathbf{U}_1 & \mathbf{U}_2 & \mathbf{U}_3 \end{vmatrix} = 2(\Omega \mathbf{U} \hat{i} - \Omega \mathbf{U}_1 \hat{k}). \quad (3.4)$$

Using Eq. (3.4), Navier-Stokes equation (2.20) in component form, become

$$\rho_{nf}(\mathbf{U}_1 \frac{\partial \mathbf{U}_1}{\partial x} + \mathbf{U}_2 \frac{\partial \mathbf{U}_1}{\partial y} + 2\Omega \mathbf{U}_3) = -\frac{\partial p^*}{\partial x} + \mu_{nf}(\frac{\partial^2 \mathbf{U}_1}{\partial x^2} + \frac{\partial^2 \mathbf{U}_1}{\partial y^2}), \quad (3.5)$$

$$\rho_{nf}(\mathbf{U}_1 \frac{\partial \mathbf{U}_2}{\partial x} + \mathbf{U}_2 \frac{\partial \mathbf{U}_2}{\partial y}) = -\frac{\partial p^*}{\partial y} + \mu_{nf}(\frac{\partial^2 \mathbf{U}_2}{\partial x^2} + \frac{\partial^2 \mathbf{U}_2}{\partial y^2}), \quad (3.6)$$

$$\rho_{nf}(\mathbf{U}_1 \frac{\partial \mathbf{U}_3}{\partial x} + \mathbf{U}_2 \frac{\partial \mathbf{U}_3}{\partial y} - 2\Omega \mathbf{U}_1) = \mu_{nf}(\frac{\partial^2 \mathbf{U}_3}{\partial x^2} + \frac{\partial^2 \mathbf{U}_3}{\partial y^2}), \quad (3.7)$$

where $p^* = p - (\frac{\Omega^2 x^2}{2})$ and $\mu_{nf} = \frac{\mu}{(1-\phi)^{2.5}}$ is the effective dynamic viscosity. The energy equation (2.26) can be written as

$$\rho C(\frac{\partial T}{\partial t} + \mathbf{U}_1 \frac{\partial T}{\partial x} + \mathbf{U}_2 \frac{\partial T}{\partial y} + \mathbf{U}_3 \frac{\partial T}{\partial z}) = k(\frac{\partial^2 T}{\partial x^2} + \frac{\partial^2 T}{\partial y^2} + \frac{\partial^2 T}{\partial z^2}). \quad (3.8)$$

For the present model, Eq. (3.8) can be represented as

$$(\mathbf{U}_1 \frac{\partial T}{\partial x} + \mathbf{U}_2 \frac{\partial T}{\partial y}) = \alpha_{nf}(\frac{\partial^2 T}{\partial x^2} + \frac{\partial^2 T}{\partial y^2}), \quad (3.9)$$

where ϕ is the volumetric fraction, $\alpha_{nf} = \frac{\kappa_{nf}}{(\rho C)_{nf}}$ is the thermal diffusivity of nanofluid,

$\rho_{nf} = (1 - \phi)\rho + \phi\rho_{cnt}$ is the effective density of the nanofluid, $(\rho C)_{nf} = (1 - \phi)\rho C + \phi(\rho C)_{cnt}$ is the heat capacity of nanofluid and the subscripts nf and cnt stands for nanofluid and carbon nanotube respectively.

The boundary conditions for the given system are

$$\mathbf{U}_1 = \mathbf{U}_v = mx, \quad \mathbf{U}_2 = 0, \quad \mathbf{U}_3 = 0, \quad T = T_a. \quad \text{at } y = 0 \quad (3.10)$$

$$\mathbf{U}_1 = 0, \quad \mathbf{U}_2 = -v_0, \quad \mathbf{U}_3 = 0, \quad T = T_0. \quad \text{at } y = h \quad (3.11)$$

At the upper wall, v_0 is the uniform suction ($v_0 > 0$) or injection ($v_0 < 0$) velocity. To transform the given system (3.5)-(3.11) to non-dimensional form, we use the following similarity transformations (see for details [19])

$$\mathbf{U}_1 = mx f'(\eta), \quad \mathbf{U}_2 = -mh f(\eta), \quad \mathbf{U}_3 = mx g(\eta), \quad \theta(\eta) = \frac{T - T_0}{T_a - T_0}, \quad \eta = \frac{y}{h}. \quad (3.12)$$

Using Eq. (3.12), various derivatives of \mathbf{U}_1 , \mathbf{U}_2 and \mathbf{U}_3 are

$$\frac{\partial \mathbf{U}_1}{\partial x} = m f'(\eta), \quad \frac{\partial \mathbf{U}_1}{\partial y} = \frac{m x f''(\eta)}{h}, \quad \frac{\partial^2 \mathbf{U}_1}{\partial y^2} = \frac{m x f'''(\eta)}{h^2}, \quad \frac{\partial^3 \mathbf{U}_1}{\partial y^3} = \frac{m x f^{(iv)}(\eta)}{h^3}, \quad (3.13)$$

$$\frac{\partial \mathbf{U}_2}{\partial x} = 0, \quad \frac{\partial \mathbf{U}_2}{\partial y} = -m f'(\eta), \quad \frac{\partial^2 \mathbf{U}_2}{\partial y^2} = \frac{-m f''(\eta)}{h}, \quad (3.14)$$

$$\frac{\partial \mathbf{U}_3}{\partial x} = 0, \quad \frac{\partial \mathbf{U}_3}{\partial y} = \frac{m x g'}{h}, \quad \frac{\partial^2 \mathbf{U}_3}{\partial y^2} = \frac{m x g''}{h^2}, \quad (3.15)$$

and those of T and θ are

$$\frac{\partial T}{\partial x} = 0, \quad \frac{\partial^2 T}{\partial x^2} = 0, \quad \frac{\partial T}{\partial y} = \frac{(T_a - T_0)\theta'}{h}, \quad \frac{\partial^2 T}{\partial y^2} = \frac{(T_a - T_0)}{h^2}\theta''. \quad (3.16)$$

Using Eqs. (3.13, 3.14), Eq. (3.3) (continuity equation) is identically satisfied. To

eliminate the pressure gradient, we take partial derivative of Eq. (3.5) and Eq. (3.6) with respect to y and x respectively

$$\rho_{nf}(\mathbf{U}_1 \frac{\partial^2 \mathbf{U}_1}{\partial y \partial x} + \frac{\partial \mathbf{U}_1}{\partial y} \frac{\partial \mathbf{U}_1}{\partial x} + \mathbf{U}_2 \frac{\partial^2 \mathbf{U}_1}{\partial y^2} + \frac{\partial \mathbf{U}_2}{\partial y} \frac{\partial \mathbf{U}_1}{\partial y} + 2\Omega \frac{\partial \mathbf{U}_3}{\partial y}) = \mu_{nf}(\frac{\partial^3 \mathbf{U}_1}{\partial y \partial x^2} + \frac{\partial^3 \mathbf{U}_1}{\partial y^3}), \quad (3.17)$$

$$\rho_{nf}(\mathbf{U}_1 \frac{\partial^2 \mathbf{U}_2}{\partial x^2} + \frac{\partial \mathbf{U}_1}{\partial x} \frac{\partial \mathbf{U}_2}{\partial x} + \mathbf{U}_1 \frac{\partial^2 \mathbf{U}_2}{\partial x \partial y} + \frac{\partial \mathbf{U}_2}{\partial x} \frac{\partial \mathbf{U}_2}{\partial y}) = \mu_{nf}(\frac{\partial^3 \mathbf{U}_2}{\partial x^3} + \frac{\partial^3 \mathbf{U}_2}{\partial x \partial y^2}), \quad (3.18)$$

By subtracting Eq. (3.17) and Eq. (3.18) and then substituting Eq. (3.13) and Eq. (3.14), we get

$$\begin{aligned} (1 - \phi)\rho + \phi\rho_{cnt} \left[+\frac{m^2 x f' f''}{h} - \frac{m^2 x f f'''}{h} + \frac{2\Omega m x g'}{h} \right] &= \frac{\mu}{(1 - \phi)^{2.5}} \left(\frac{m x f^{(iv)}}{h^3} \right), \\ \left[(1 - \phi) + \frac{\phi\rho_{cnt}}{\rho} \right] (1 - \phi)^{2.5} \left[\frac{m^2 x f' f''}{h} - \frac{m^2 x f f'''}{h} + \frac{2\Omega m x g'}{h} \right] &= \frac{\mu}{\rho} \left(\frac{m x f^{(iv)}}{h^3} \right), \\ \varepsilon_1 [m^2 x f' f'' - m^2 x f f'''] + 2\Omega m x g' &= \nu \left(\frac{m x f^{iv}}{h^2} \right), \\ \left(\frac{h^2}{\nu} \right) \varepsilon_1 [m^2 x f' f'' - m^2 x f f'''] + 2\Omega m x g' &= m x f^{(iv)}, \\ f^{(iv)} - \varepsilon_1 A_1 (f' f'' - f f''') - 2\varepsilon_1 A_2 g' &= 0. \end{aligned} \quad (3.19)$$

Here A_1 and A_2 are dimensionless parameters which are defined as

$$\begin{aligned} A_1 &= \frac{m h^2}{\nu}, \quad (\text{Reynolds number}) \quad A_2 = \frac{\Omega h^2}{\nu}, \quad (\text{Rotation parameter}) \\ \varepsilon_1 &= \left[(1 - \phi) + \phi \frac{\rho_{cnt}}{\rho} \right] (1 - \phi)^{2.5}. \end{aligned} \quad (3.20)$$

Similarly substituting Eq. (3.15) in Eq. (3.6), we have

$$\begin{aligned}
(1 - \phi)\rho + \phi\rho_{cnt} \left[(mxf')(mg) + (-mhf)\left(\frac{mxg'}{h}\right) - 2\Omega mxf' \right] &= \frac{\mu}{(1 - \phi)^{2.5}} \left(\frac{mxg''}{h^2}\right), \\
\left[(1 - \phi) + \frac{\phi\rho_{cnt}}{\rho} \right] (1 - \phi)^{2.5} [m^2xf'g - m^2fxg' - 2\Omega mxf'] &= \frac{\mu}{\rho} \left(\frac{mxg''}{h^2}\right), \\
\varepsilon_1 [m^2xf'g - m^2fxg' - 2\Omega mxf'] &= \nu \left(\frac{mxg''}{h^2}\right), \\
\varepsilon_1 \left(\frac{\nu}{h^2}\right) [m^2xf'g - m^2fxg' - 2\Omega mxf'] &= mxg'', \\
\varepsilon_1 A_1 (gf' - fg') - 2\Omega mxf' &= g'', \\
g'' - \varepsilon_1 A_1 (gf' - fg') + 2\varepsilon_1 A_2 f' &= 0.
\end{aligned} \tag{3.21}$$

Further substituting Eq. (3.16) in Eq. (3.9) gives

$$\begin{aligned}
[0 + -mhf\left(\frac{T_a - T_0}{h}\right)\theta'] &= \frac{\kappa_{nf}}{(\rho C)_{nf}} \left(\frac{T_a - T_0}{h^2}\right)\theta'', \\
\theta'' + \frac{mh^2 f(\eta) f'(\rho C)_{nf}}{\kappa_{nf}} &= 0, \\
\theta'' + \left[\frac{mh^2 (\rho C)_{nf}}{\nu \kappa} \frac{1}{\frac{\kappa_{nf}}{\kappa \nu}} \right] f(\eta) \theta' &= 0, \\
\theta'' + \left[\frac{A_1 \nu}{\varepsilon_3 \kappa} ((1 - \phi)\rho Cp + \phi(\rho C)_{cnt}) \right] f(\eta) \theta' &= 0, \\
\theta'' \left[\frac{A_1 \nu \varepsilon_2 (\rho Cp)}{\varepsilon_3 \kappa} \right] f(\eta) \theta' &= 0, \\
\theta'' + \frac{A_1}{\varepsilon_3} \varepsilon_2 Pr f(\eta) \theta' &= 0,
\end{aligned} \tag{3.22}$$

where,

$$\varepsilon_2 = \left[(1 - \phi) + \phi \frac{(\rho C)_{cnt}}{\rho C} \right], \tag{3.23}$$

$$\varepsilon_3 = \frac{\kappa_{nf}}{\kappa} = \frac{1 - \phi + 2\phi \left(\frac{\kappa_{cnt}}{\kappa_{cnt} - \kappa}\right) \ln\left(\frac{\kappa_{cnt} + \kappa}{2\kappa}\right)}{1 - \phi + 2\phi \left(\frac{\kappa}{\kappa_{cnt} - \kappa}\right) \ln\left(\frac{\kappa_{cnt} + \kappa}{2\kappa}\right)}. \tag{3.24}$$

Here Eqs. (3.19-3.22) are the non-dimensional system of ordinary differential equations along with the following non-dimensional boundary conditions.

at $\eta = 0$ (corresponding to $y = 0$, from Eq. (3.10) and use of Eq. (3.12))

$$g(0) = 0, \quad \theta(0) = 1, \quad f(0) = 0, \quad f'(0) = 1. \quad (3.25)$$

at $\eta = 1$ (corresponding to $y = h$, from Eq. (3.11) and use of Eq. (3.12))

$$g(1) = 0, \quad \theta(1) = 0, \quad f(1) = S, \quad f'(1) = 0. \quad (3.26)$$

where S is the suction/injection parameter.

The important physical parameters of skin friction coefficient and local Nusselt number, in terms of nanofluid properties (see details in [2]) are

$$C_f = \frac{\tau_v}{\rho_{nf} U_v^2}, \quad (3.27)$$

$$Nu = \frac{x q_v}{\kappa_{nf} (T_a - T_0)}, \quad (3.28)$$

where $\tau_v = \mu_{nf} \frac{\partial u}{\partial y}$ is the shear stress and $q_v = -\kappa_{nf} \frac{\partial T}{\partial y}$ is the heat flux. Using similarity transformations from Eq. (3.12), Eq. (3.27) and Eq. (3.28) give

$$C_f^* = \frac{U_v h}{\nu_f} C_f = \frac{f''(\eta)}{\left(\frac{1}{(1-\phi) + \phi \frac{\rho_{cnt}}{\rho}} \right) (1-\phi)^{2.5}}, \quad (3.29)$$

$$Nu_x^* = \frac{h}{x} Nu_x = -\theta'(\eta), \quad (3.30)$$

at $\eta = 0$ and $\eta = 1$.

3.2 Results and Discussion

A built-in solver *bvp4c* (MATLAB) is used to numerically solve the problem given by Eq. (3.19-3.22) with boundary conditions Eqs. (3.25, 3.26), then the effect of different parameters (suction/injection (S), nanoparticle volume fraction (ϕ), Reynolds number (A_1) and rotation (A_2)) on SW_{CNT} and MW_{CNT} are presented graphically. Thermophysical properties of base fluid (water) and CNTs (Haq et. al [23]) are given in Table 3.1

Physical properties	Base fluid (water)	MW_{CNT}	SW_{CNT}
Pr	6.2		
κ	0.613	3000	6600
ρ	997	1600	2600
C_p	4179	796	425

Table 3.1: Thermophysical properties of base fluid and carbon nanotubes.

3.2.1 Velocity and Temperature

In Fig. 3.2(a), with increasing value of volume fraction ϕ , $f'(\eta)$ also increases. However there is a minor diversity in velocity profile, velocity of SW_{CNT} is lower as compared to MW_{CNT} . Figure 3.2(b) shows variation of $g(\eta)$ with different values of ϕ and it is observed that SW_{CNT} have high velocity profile in comparison with MW_{CNT} . Moreover velocity $g(\eta)$ decreases with increasing values of nanoparticles volume fraction. Figure 3.2(c) shows an increase in $\theta(\eta)$ with increasing values of ϕ , which is due to more resistance between fluid and sheet. In this case, both SW_{CNT} and MW_{CNT} have nearly same temperature profile.

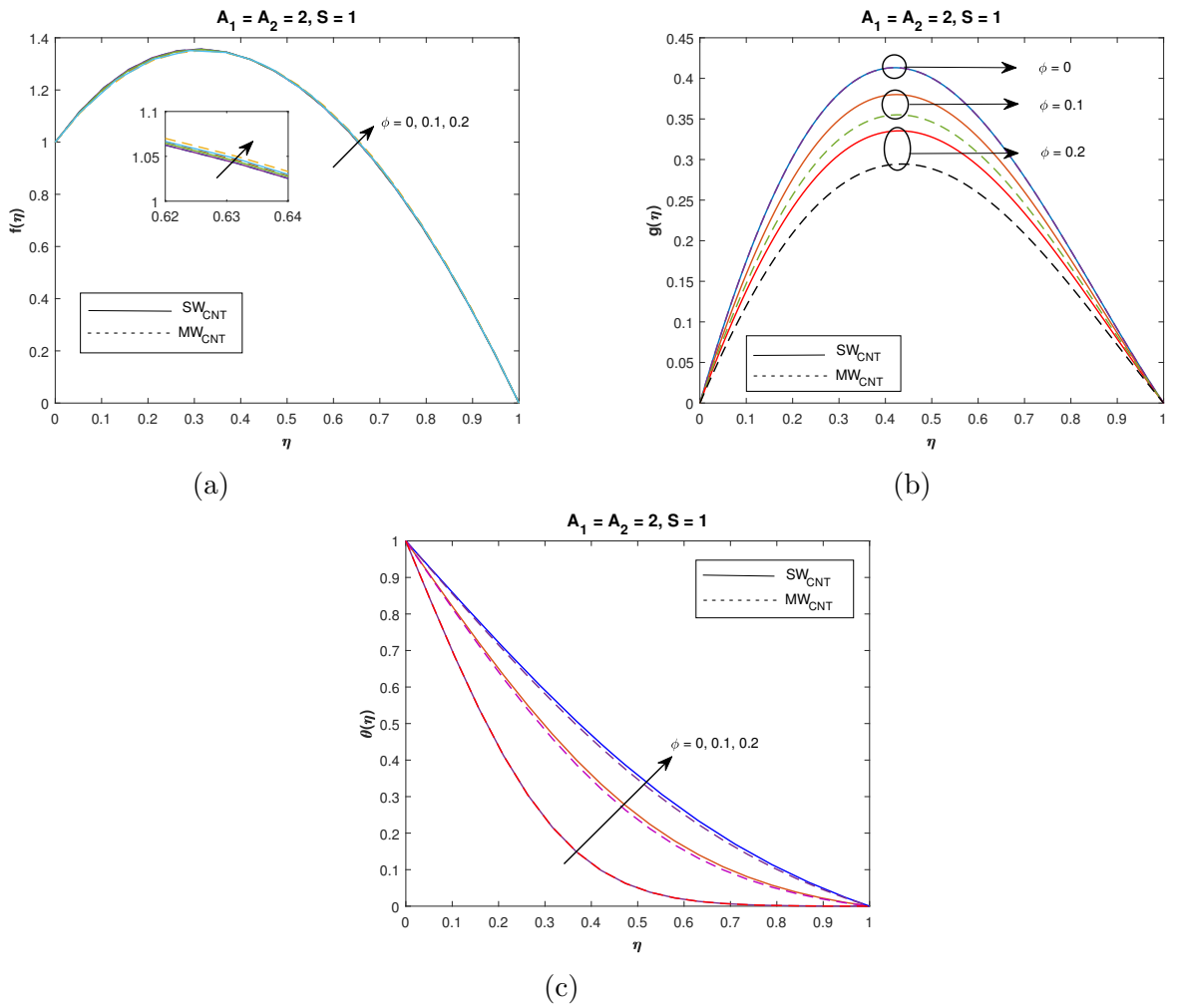


Figure 3.2: Velocity variation in (a-b) and temperature in (c) with respect to η for diverse choices of ϕ .

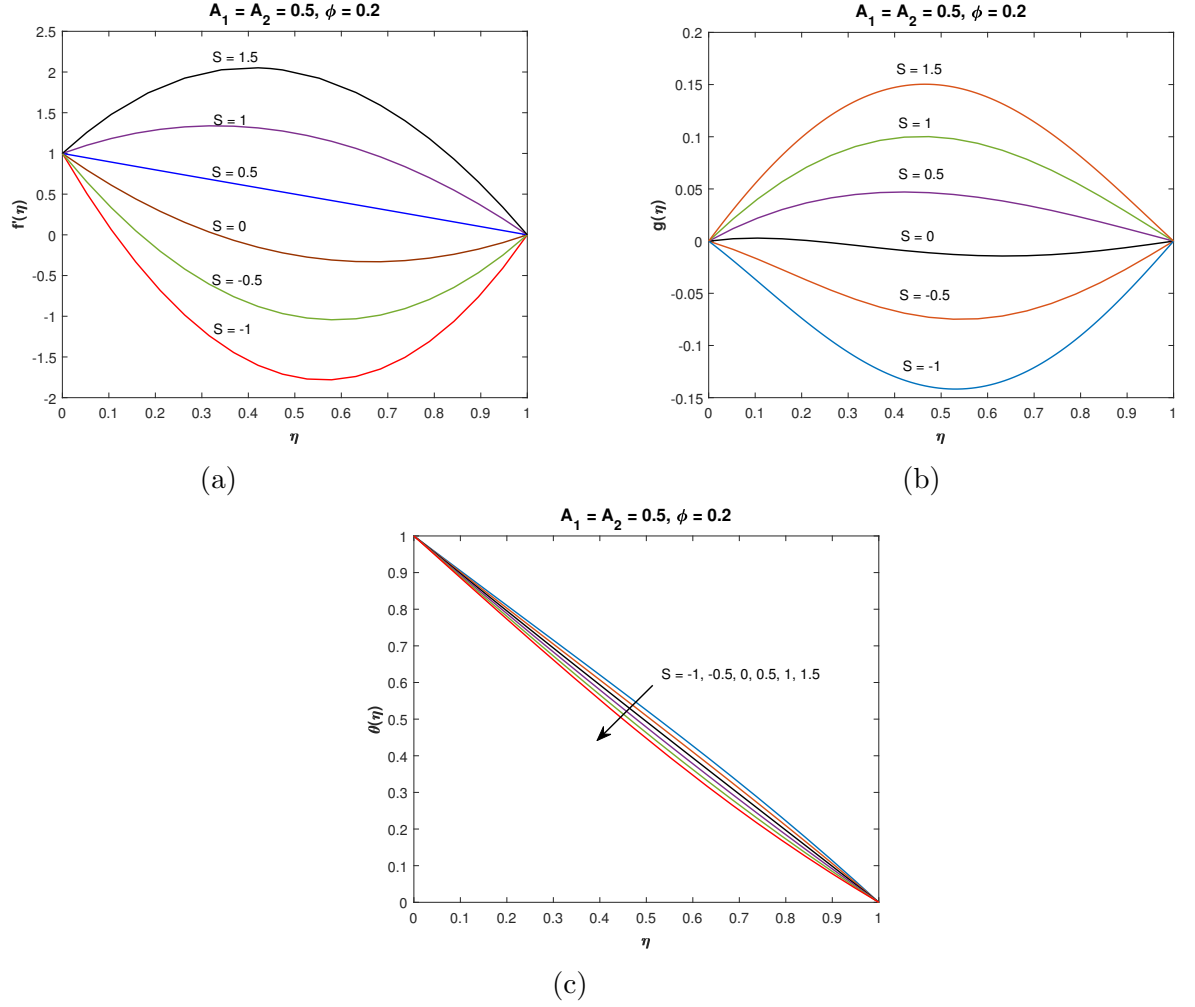


Figure 3.3: Velocity variation in (a-b) and temperature in (c) with respect to η for diverse choices of S .

Figures (3.3)-(3.5) are plotted for $f'(\eta)$, $g(\eta)$ and $\theta(\eta)$ for varying values of suction/injection parameter (S), Reynolds number (A_1) and rotation parameter (A_2) for SW_{CNT} respectively.

Figures 3.3(a-b) demonstrate that both velocity profiles $f'(\eta)$ and $g(\eta)$ increase with increasing values of S . As compared to the upper and lower plates of the channel, these differences in the velocities are more notable at the mean position. Figure 3.3(c) depicts that when values of S increase, temperature profile θ decreases.

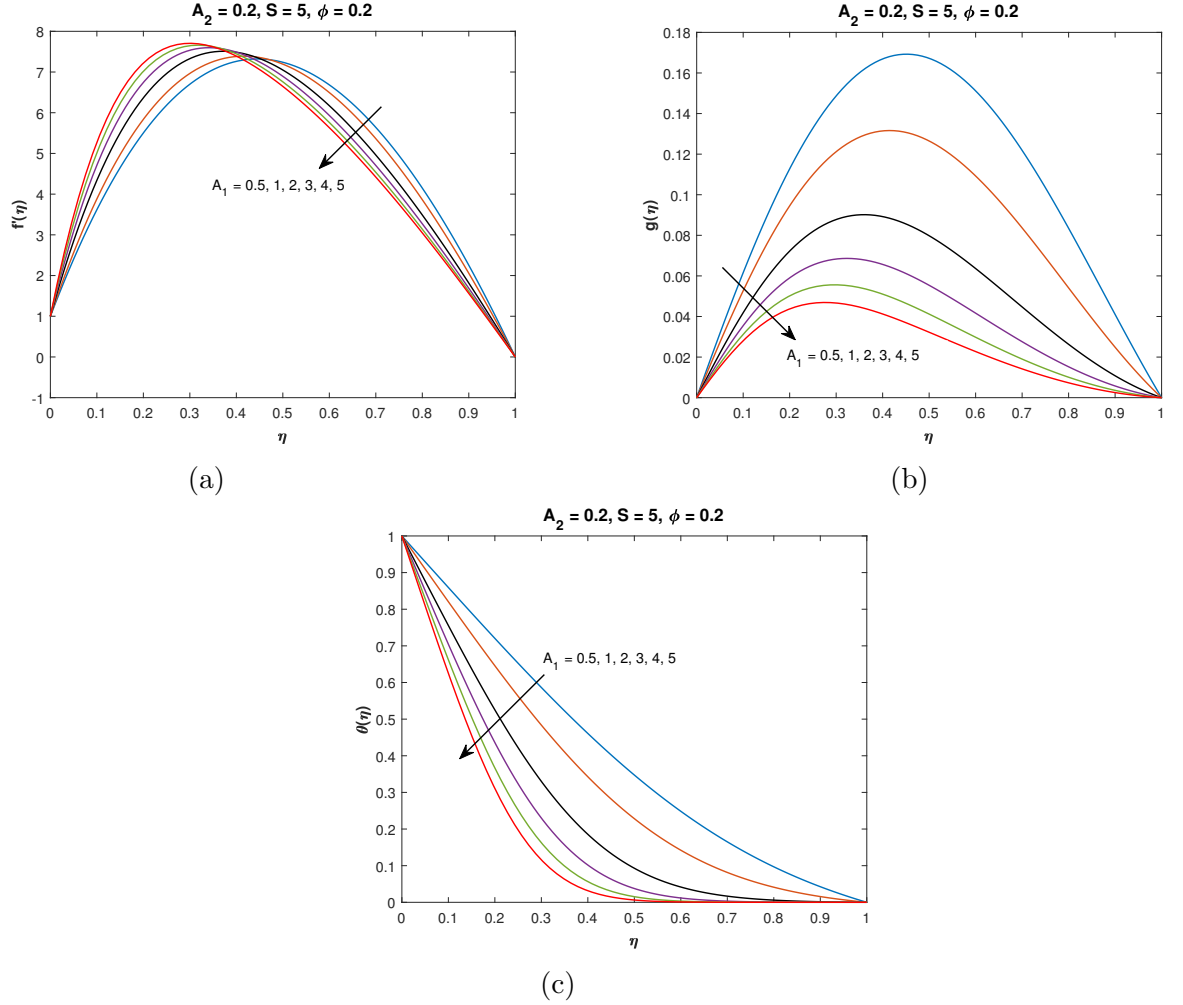


Figure 3.4: Velocity variation in (a-b) and temperature in (c) with respect to η for diverse choices of A_1 .

In Fig. 3.4(a), with the increasing values of Reynolds number A_1 , the velocity profile $f'(\eta)$ changes its behavior in ascending order at the mean position due to the stretching effect of lower plate. In Fig. 3.4(b) $g(\eta)$ decreases, as value of A_1 rises. When the lower plate is at static position, the peak value of $g(\eta)$ is shifted towards the lower plate. In Fig. 3.4(c), temperature profile ($\theta(\eta)$) falls as the value of A_1 rises.

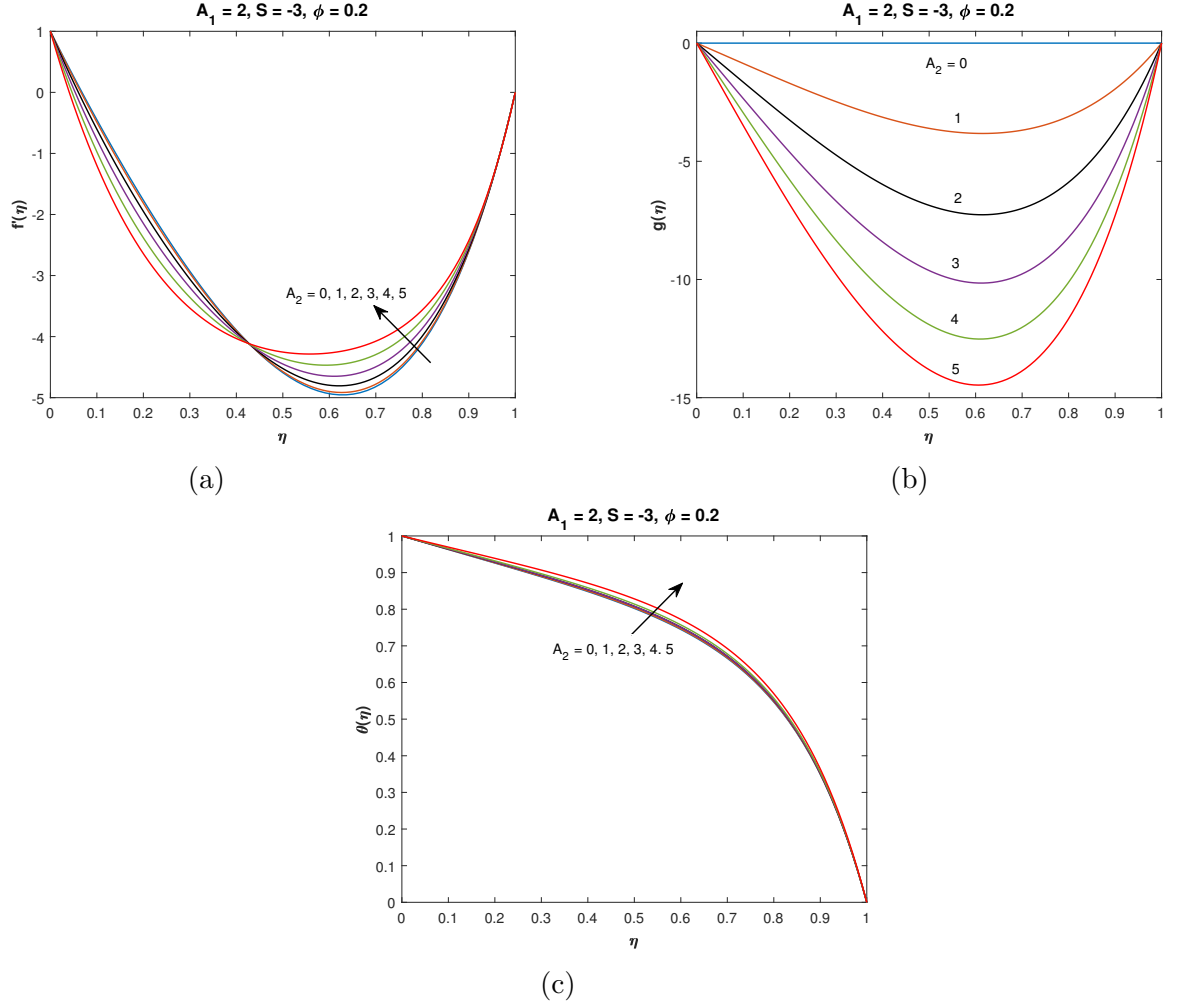


Figure 3.5: Velocity variation in (a-b) and temperature in (c) with respect to η for diverse choices of A_2 .

In Fig. 3.5(a), $f'(\eta)$ is decreasing with rising values of rotation parameter (A_2) but this decreasing behavior of $f'(\eta)$ is of dual nature. Figure 3.5(b) shows a decreasing behavior of $g(\eta)$ but in comparison to lower and upper wall velocity variation is higher at mean position. The problem is reduced to two-dimensional flow in a channel, without the rotation parameter $A_2 = 0$ (z -component of the velocity). In Fig. 3.5(c), temperature profile θ is increasing with the rising values of rotation parameter A_2 .

3.2.2 Local Nusselt number and the skin friction coefficient

The skin friction coefficient and the local nusselt number behavior for different parameters is observed in this section. Prior to graphical discussion, Tables (3.1)-(3.4) are constructed in which different values of C_f^* (Eq. 3.29) and Nu_x^* (Eq. 3.30) are obtained for increasing choices of Reynolds number (A_1), rotation parameter (A_2), nanoparticle volume fraction (ϕ) and suction / injection parameter (S).

S	ϕ	$A_2 = 0$		$A_2 = 0.5$		$A_2 = 1$	
		$A_1 = 0.5$	$A_1 = 1$	$A_1 = 0.5$	$A_1 = 1$	$A_1 = 0.5$	$A_1 = 1$
1	0	2.10694	2.21327	2.1137	2.21887	2.13398	2.23565
	0.1	2.34916	2.45562	2.35531	2.46081	2.37377	2.47642
	0.2	2.75073	2.85732	2.75608	2.86197	2.77213	2.8759
0	0	-4.04282	-4.08556	-4.04541	-4.08816	-4.05316	-4.09595
	0.1	-4.52721	-4.56997	-4.52952	-4.57228	-4.53643	-4.57922
	0.2	-5.33028	-5.37306	-5.33224	-5.37502	-5.33811	-5.3809
-1	0	-9.73486	-9.46811	-9.75041	-9.48649	-9.79701	-9.54155
	0.1	-10.9459	-10.6794	-10.9595	-10.6952	-11.0004	-10.7426
	0.2	-12.9537	-12.6875	-12.965	-12.7003	-12.9989	-12.7387

Table 3.2: Numerical values of the skin friction coefficient (Eq. (3.29)) at $\eta = 0$ against different parameters.

In Table 3.2, when $S = 1$, C_f^* is showing an increasing behavior for increasing values of ϕ , A_1 and A_2 but for $S = -1$ and 0 , its value falls. For fixed value S ($S > 0$), ϕ and A_1 , for increasing values of rotation parameter (A_2), value of C_f^* increases.

S	ϕ	$A_2 = 0$		$A_2 = 0.5$		$A_2 = 1$	
		$A_1 = 0.5$	$A_1 = 1$	$A_1 = 0.5$	$A_1 = 1$	$A_1 = 0.5$	$A_1 = 1$
1	0	-3.88037	-3.77309	-3.89058	-3.78257	-3.92117	-3.81099
	0.1	-4.36407	-4.25487	-4.37324	-4.26347	-4.40075	-4.28925
	0.2	-5.16626	-5.05463	-5.17412	-5.06207	-5.19767	-5.08438
0	0	1.97639	1.95318	1.97626	1.95311	1.97585	1.95289
	0.1	2.21856	2.19529	2.21844	2.19521	2.21806	2.19498
	0.2	2.62007	2.59671	2.61996	2.59663	2.61962	2.5964
-1	0	8.3863	8.80893	8.39761	8.82109	8.4315	8.85752
	0.1	9.35315	9.7697	9.36315	9.78037	9.39315	9.81237
	0.2	10.9569	11.3659	10.9653	11.3748	10.9905	11.4014

Table 3.3: Numerical values of the skin friction coefficient (Eq. (3.29)) at $\eta = 1$ against different parameters.

In Table 3.3, behavior of C_f^* is opposite to that found in Table (3.2). When $S = 1$, C_f^* is decreasing with rising values of ϕ , A_1 and A_2 but it rises for $S = -1$ and 0.

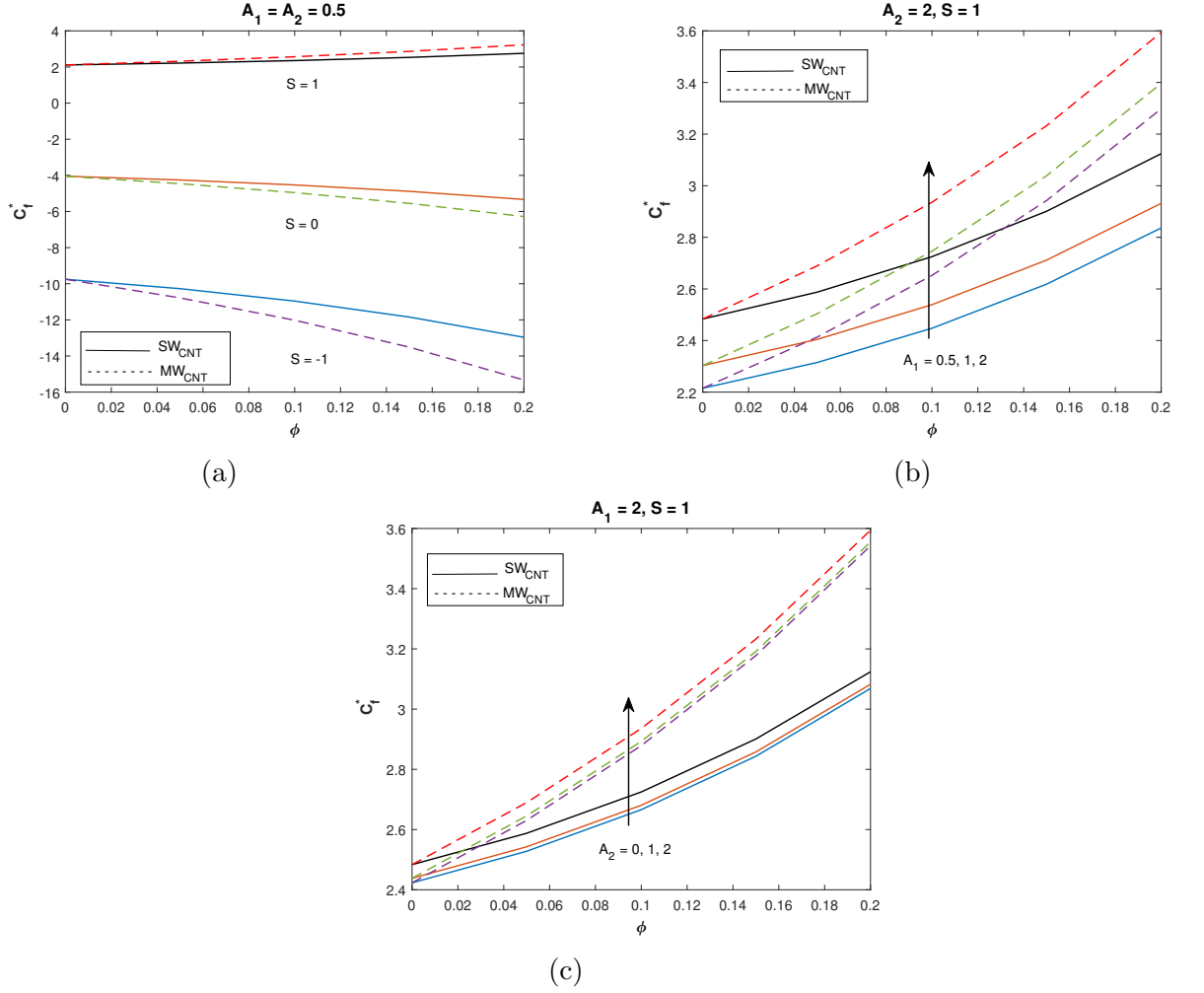


Figure 3.6: Fluctuation of the skin friction coefficient (Eq. (3.29)) at $\eta = 0$ for SW_{CNT} and MW_{CNT} against different values of S , A_1 and A_2 .

For the skin friction, the comparisons between SW_{CNT} and MW_{CNT} with different parameters are shown graphically in Fig. 3.6 and 3.7 for $\eta = 0$ and $\eta = 1$ respectively. Figure 3.6(a) shows C_f^* at lower wall for diverse values of suction/injection parameter S . For $S = 1$, SW_{CNT} and MW_{CNT} behaves differently as compared to $S = 0$ and -1 . In Fig. 3.6(b-c) C_f^* is plotted for varying Reynolds number and rotation parameters (A_1 and A_2). In both cases there is an increasing behavior. In comparison to SW_{CNT} , MW_{CNT} have higher C_f^* .

In Fig. 3.7(a) we can observe C_f^* at upper wall for different suction parameter S . For $S = -1$ and 0 , C_f^* is increasing but for $S = 1$, its behavior is opposite. In case of rotation parameter A_2 (Fig. 3.7(b)), behavior of C_f^* at the upper wall is same as it was at the lower wall. In Fig. 3.7(c), the value of C_f^* is decreasing for increasing values of A_1 .

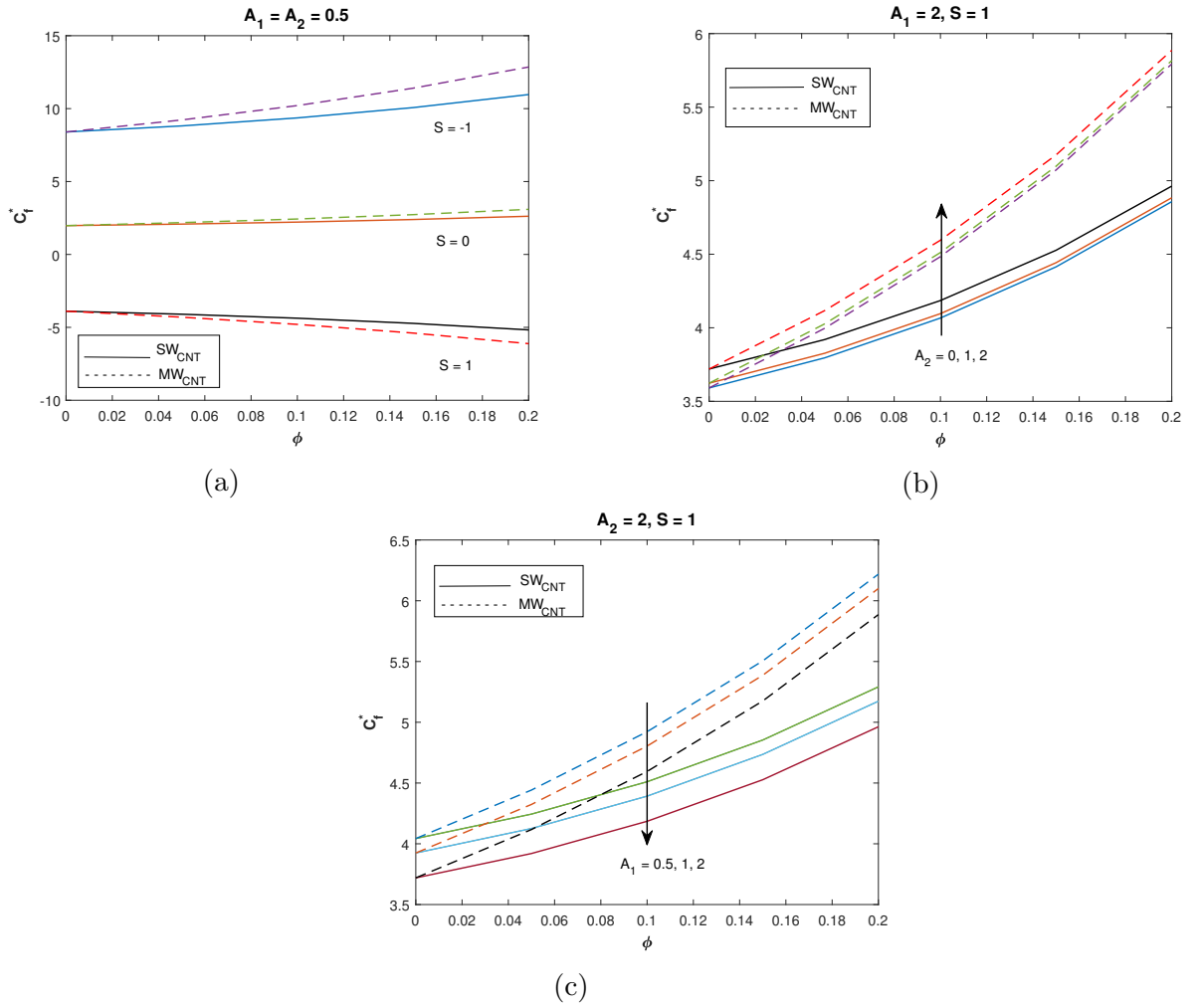


Figure 3.7: Fluctuation of the skin friction coefficient (Eq. (3.29)) at $\eta = 1$ for SW_{CNT} and MW_{CNT} against different values of S , A_1 and A_2 .

S	ϕ	$A_2 = 0$		$A_2 = 0.5$		$A_2 = 1$	
		$A_1 = 0.5$	$A_1 = 1$	$A_1 = 0.5$	$A_1 = 1$	$A_1 = 0.5$	$A_1 = 1$
-1	0	0.679525	0.390749	0.679423	0.390567	0.679116	0.390023
	0.1	0.900872	0.802434	0.900841	0.822358	0.900749	0.802129
	0.2	0.950328	0.901409	0.950317	0.901381	0.950284	0.901298
0	0	1.161852	1.336615	1.161792	1.336485	1.161611	1.336104
	0.1	1.049929	1.100939	1.049914	1.10091	1.049871	1.100822
	0.2	1.02508	1.050363	1.0205075	1.050353	1.025059	1.050322
1	0	1.628938	2.195148	1.628918	2.195110	1.628859	2.194999
	0.1	1.201080	1.405087	1.201072	1.405066	1.201049	1.405002
	0.2	1.101123	1.204080	1.101120	1.204072	1.101112	1.204048

Table 3.4: Numerical values of local Nusselt number (Eq. (3.30)) at $\eta = 0$ against different parameters.

S	ϕ	$A_2 = 0$		$A_2 = 0.5$		$A_2 = 1$	
		$A_1 = 0.5$	$A_1 = 1$	$A_1 = 0.5$	$A_1 = 1$	$A_1 = 0.5$	$A_1 = 1$
-1	0	2.430376	4.822166	2.430418	4.822362	2.430543	4.822943
	0.1	1.352946	1.791098	1.352954	1.791140	1.352978	1.791262
	0.2	1.167787	1.355238	1.167790	1.355249	1.167797	1.35528
0	0	0.898716	0.802164	0.898759	0.802245	0.89889	0.802489
	0.1	0.967408	0.935499	0.967426	0.935521	0.967453	0.935587
	0.2	0.983468	0.967174	0.983472	0.967185	0.983484	0.967209
1	0	0.265509	0.057693	0.265542	0.057711	0.265642	0.057765
	0.1	0.674365	0.441207	0.674384	0.441236	0.674439	0.441322
	0.2	0.822230	0.670448	0.822238	0.670462	0.822261	0.670505

Table 3.5: Numerical values of local Nusselt number (Eq. (3.30)) at $\eta = 1$ against different parameters.

In Table 3.4, when $S = 1$, value of Nu_x^* is increasing with increasing values of ϕ , A_1 and A_2 but for $S = -1, 0$ it is decreasing. But at $\eta = 1$, its behavior is totally opposite, as is obvious from Table 3.5

For the local Nusselt number, the comparison between SW_{CNT} and MW_{CNT} with different parameters are shown graphically.

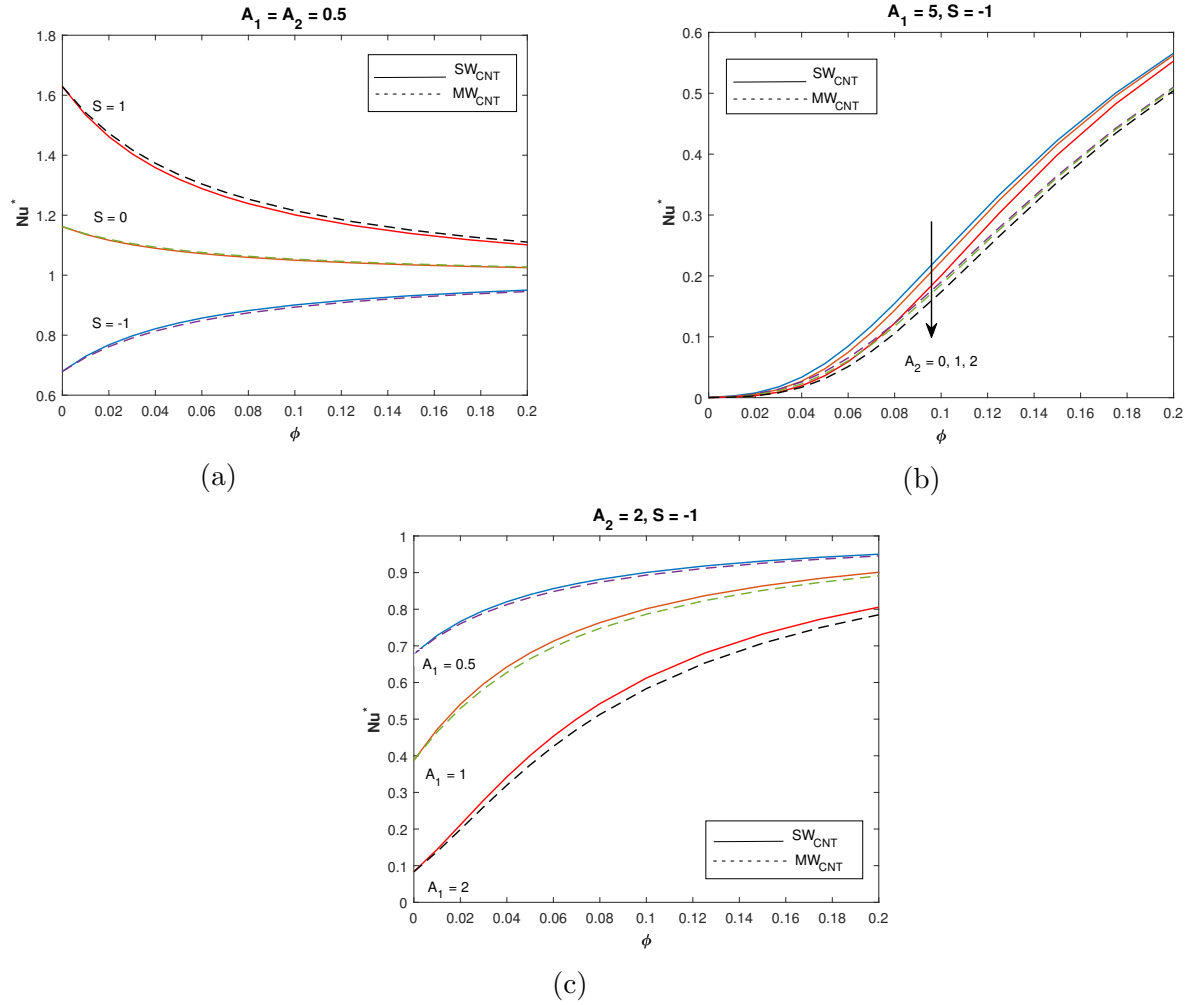


Figure 3.8: Fluctuation of local Nusselt number (Eq. (3.30)) at $\eta = 0$ for SW_{CNT} and MW_{CNT} against different choices of S , A_1 and A_2 .

Figure 3.8(a) depicts Nu_x^* at the lower wall for different values of S . With the increasing values of nanoparticle volume fraction ϕ , Nu_x^* is decreasing but for $S = -1$ it shows an increasing behavior. In Fig. 3.8(b-c) graphs are plotted for Reynolds number (A_1) and rotation parameter (A_2) respectively. It is observed that increasing the Reynolds number and rotational speed causes an increase in heat transfer rate.

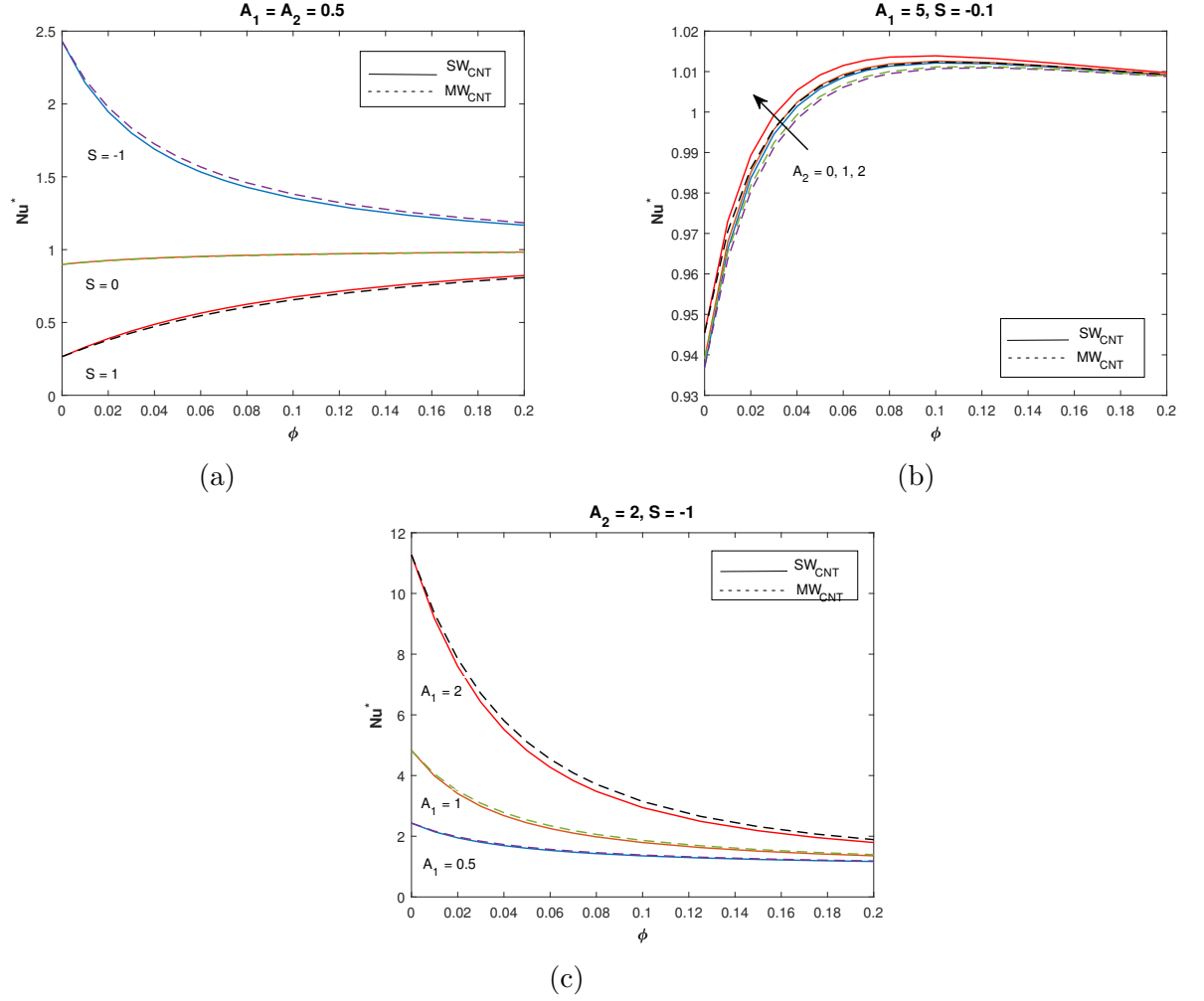


Figure 3.9: Fluctuation of local Nusselt number (Eq. 3.30) at $\eta = 1$ for SW_{CNT} and MW_{CNT} against different choices of S , A_1 and A_2 .

Figure 3.9 (a) and (c) demonstrates that with the increase in the suction/injection parameter (S) and rotation parameter (A_2), Nu_x^* increases but in Fig. 3.9(b) case is different. The value of Nu_x^* decreases with increasing Reynolds number. SW_{CNT} have high heat transfer rate as compared to MW_{CNT} . In case of A_1 , A_2 and $S = -1$, with the rising value of ϕ , Nu_x^* rises but for $S = 0, 1$ its value falls.

Chapter 4

Thermal radiation and heat source effect on MHD flow of carbon nanotubes in a rotating channel

The effect of thermal radiation and the heat source on flow of C_{NT} in a rotating channel, in the presence of magnetic field is investigated in this chapter. Using similarity transformations, non-linear ordinary differential equations are obtained from governing partial differential equations. Numerical solutions for velocity profile, temperature profile, local Nusselt number and the skin friction coefficient are obtained by using *bvp4c*, solver of MATLAB. Graphs are presented to explore the physical behaviors of relevant parameters on the flow and heat transfer characteristics.

4.1 Mathematical formulation

Consider a steady, incompressible rotating flow of C_{NT} , with water as base fluid, between two infinite plates. The variable velocity of the lower plate is of the form $\mathbf{U}_v = mx(m > 0)$ while the upper plate is porous. To uniformly access the motion of C_{NT} , a uniform magnetic field B_0 is applied in direction of y-axis. \mathbf{U}_1 , \mathbf{U}_2 and \mathbf{U}_3 are the components of velocity in x , y and z directions respectively.

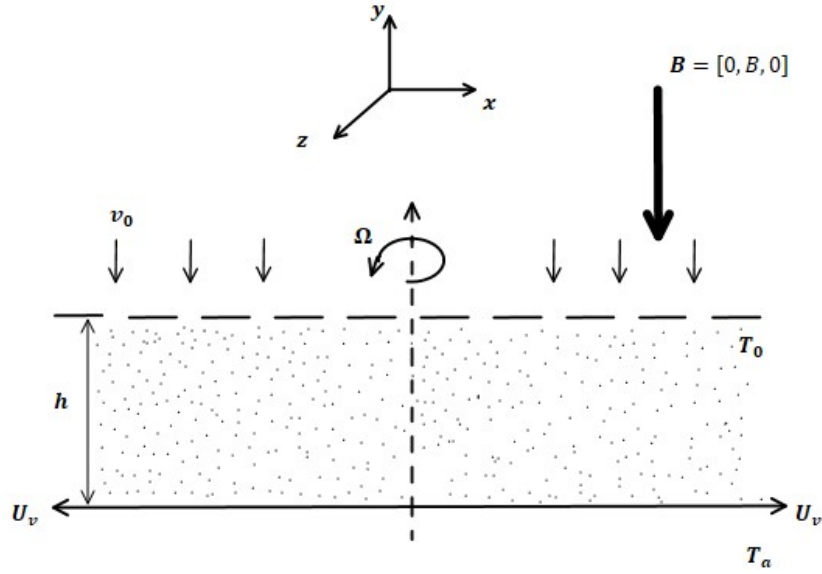


Figure 4.1: Flow field geometry

The governing continuity, momentum and thermal energy partial differential equations for the given MHD flow are

$$\frac{\partial \mathbf{U}_1}{\partial x} + \frac{\partial \mathbf{U}_2}{\partial y} = 0, \quad (4.1)$$

$$\rho_{nf}(\mathbf{U}_1 \frac{\partial \mathbf{U}_1}{\partial x} + \mathbf{U}_2 \frac{\partial \mathbf{U}_1}{\partial y} + 2\Omega \mathbf{U}_3) = -\frac{\partial p^*}{\partial x} + \mu_{nf}(\frac{\partial^2 \mathbf{U}_1}{\partial x^2} + \frac{\partial^2 \mathbf{U}_1}{\partial y^2}) - \sigma B_0^2 \mathbf{U}_1, \quad (4.2)$$

$$\rho_{nf}(\mathbf{U}_1 \frac{\partial \mathbf{U}_2}{\partial x} + \mathbf{U}_2 \frac{\partial \mathbf{U}_2}{\partial y}) = -\frac{\partial p^*}{\partial y} + \mu_{nf}(\frac{\partial^2 \mathbf{U}_2}{\partial x^2} + \frac{\partial^2 \mathbf{U}_2}{\partial y^2}), \quad (4.3)$$

$$\rho_{nf}(\mathbf{U}_1 \frac{\partial \mathbf{U}_3}{\partial x} + U_2 \frac{\partial \mathbf{U}_3}{\partial y} - 2\Omega \mathbf{U}_1) = \mu_{nf}(\frac{\partial^2 \mathbf{U}_3}{\partial x^2} + \frac{\partial^2 \mathbf{U}_3}{\partial y^2}) - \sigma B_0^2 \mathbf{U}_3, \quad (4.4)$$

where, $p^* = p - (\frac{\Omega x^2}{2})$, μ_{nf} is the dynamic viscosity of nanofluids, ρ_{nf} is the effective density of nanofluid and the subscripts nf stands for nanofluids.

The thermal energy partial differential equation is:

$$(\rho C)_{nf}(\mathbf{U}_1 \frac{\partial T}{\partial x} + \mathbf{U}_2 \frac{\partial T}{\partial y}) = \kappa_{nf}(\frac{\partial^2 T}{\partial x^2} + \frac{\partial^2 T}{\partial y^2}) - \frac{\partial q_r}{\partial y} + Q_0(T - T_a). \quad (4.5)$$

where $(\rho C)_{nf} = (1 - \phi)\rho C + \phi(\rho C)_{cnt}$ is the heat capacity of nanofluid, $q_r = -\frac{4\sigma^* T_a^4}{3k^*}$ is the radiative heat flux [24], σ^* is Stefan Boltzman constant, k^* is the mean absorption coefficient and Q_0 is the heat source parameter.

The initial and boundary conditions for the given problem are:

$$\begin{aligned} \mathbf{U}_1 = \mathbf{U}_v = mx, \quad \mathbf{U}_2 = \mathbf{U}_3 = 0, \quad T = T_a, \quad \text{at } y = 0, \\ \mathbf{U}_1 = 0, \quad \mathbf{U}_2 = -v_0, \quad \mathbf{U}_3 = 0, \quad -\kappa \frac{\partial T}{\partial y} = h[T - T_a], \quad \text{at } y = h. \end{aligned} \quad (4.6)$$

where κ , h and v_0 represents the thermal conductivity, convective heat transfer coefficient and the uniform suction/injection velocity. The last boundary condition in Eq. (4.6) is due to Newton's law of cooling.

Following similarity transformations are used to obtain non-dimensional system of equations (4.1-4.6) [19]

$$\mathbf{U}_1 = mx f'(\eta), \quad \mathbf{U}_2 = -mh f(\eta), \quad \mathbf{U}_3 = mx g(\eta), \quad \theta(\eta) = \frac{T - T_0}{T_a - T_0}, \quad \eta = \frac{y}{h}. \quad (4.7)$$

Equation (4.1) (equation of continuity) is satisfied identically. To eliminate the partial derivative of p^* , we take the y derivative of Eq. (4.2) and x derivative of Eq. (4.3).

The resultant equations are subtracted and we arrive at a single equation, after using Eq. (4.7) this becomes

$$(1 - \phi)\rho + \phi\rho_{Cnt}\left[\frac{m^2xf'f''}{h} - \frac{m^2xf f'''}{h} + \frac{2\Omega mxg'}{h}\right] = \frac{\mu}{(1 - \phi)^{2.5}}\left(\frac{mxf^{iv}}{h^3}\right) - \sigma B_0^2 mxf'',$$

$$\left[(1 - \phi) + \frac{\phi\rho_{Cnt}}{\rho}\right](1 - \phi)^{2.5}\left[\frac{m^2xf'f''}{h} - \frac{m^2xf f'''}{h} + \frac{2\Omega mxg'}{h}\right] = \frac{\mu}{\rho}\left(\frac{mxf^{iv}}{h^3}\right),$$

$$- \frac{\sigma}{\rho} B_0^2 mxf''(1 - \phi)^{2.5},$$

$$\varepsilon_1[m^2xf'f'' - m^2xf f''' + 2\Omega mxg'] = \nu\left(\frac{mxf^{iv}}{h^2}\right) - \frac{\sigma}{\rho} B_0^2 mxf''(1 - \phi)^{2.5},$$

$$\left(\frac{h^2}{\nu}\right)\varepsilon_1[m^2xf'f'' - m^2xf f''' + 2\Omega mxg'] = mxf^{iv} - \frac{\sigma h^2}{\rho\nu} B_0^2 mxf''(1 - \phi)^{2.5},$$

$$f^{iv} - \varepsilon_1 A_1(f'f'' - f f''') - 2A_2\varepsilon_1 g' - Mf'' = 0. \quad (4.8)$$

Here A_1 is the Reynolds number, A_2 is rotation parameter and M is the magnetic parameter.

$$A_1 = \frac{mh^2}{\nu}, \quad A_2 = \frac{\Omega h^2}{\nu}, \quad \varepsilon_1 = \left[(1 - \phi) + \phi\frac{\rho_{Cnt}}{\rho}\right](1 - \phi)^{2.5}, \quad M = \frac{\sigma h^2 B_0^2}{\rho\nu}(1 - \phi)^{2.5}, \quad (4.9)$$

Substituting Eq. (4.7) in Eq. (4.4), the differential equation in $g(\eta)$ is obtained as

$$\left[(1 - \phi) + \frac{\phi\rho_{Cnt}}{\rho}\right](1 - \phi)^{2.5}[m^2xf'g - m^2fxg' - 2\Omega mx f'] = \frac{\mu}{\rho}\left(\frac{m x g''}{h^2}\right)B^2$$

$$- \frac{\sigma}{\rho_0} m x g(1 - \phi)^{2.5},$$

$$\begin{aligned}
\varepsilon_1[m^2 x f' g - m^2 f x g' - 2\Omega m x f'] &= \nu \left(\frac{m x g''}{h^2} \right) - \frac{\sigma}{\rho} B_0^2 m x g (1 - \phi)^{2.5}, \\
\varepsilon_1 \left(\frac{\nu}{h^2} \right) [m^2 x f' g - m^2 f x g' - 2\Omega m x f'] &+ \frac{\sigma h^2}{\rho \nu} B_0^2 m x g (1 - \phi)^{2.5} = m x g'', \\
g'' - \varepsilon_1 A_1 (g f' - f g') + 2\varepsilon_1 A_2 f' - M g &= 0.
\end{aligned} \tag{4.10}$$

substitution of Eq. (4.7) in Eq. (4.5) gives

$$\begin{aligned}
- m f \theta' &= \frac{\kappa_{nf}}{(\rho C)_{nf} h^2} \theta'' + \frac{16\sigma^*}{3\kappa^*} \frac{T_a^3}{(\rho C)_{nf}} \theta'' + \frac{Q_0}{(\rho C)_{nf}} \theta, \\
- \left(\frac{(\rho C)_{nf}}{\kappa_{nf}} \right) m f h^2 \theta' - \frac{Q_0 h^2}{\kappa_{nf}} \theta - \theta'' \left(1 + \frac{16\sigma^* T_a^3}{3\kappa^* \kappa_{nf}} \right) &= 0, \\
\left[\frac{m h^2 \nu (\rho C)_{nf}}{\nu \kappa} \frac{1}{\frac{\kappa_{nf}}{\kappa}} \right] f(\eta) \theta' + \frac{Q_0 h^2}{\frac{\kappa_{nf}}{\kappa} \kappa} \theta + \theta'' \left(1 + \frac{16\sigma}{3\kappa^*} \frac{T_a^3}{\frac{\kappa_{nf} \kappa}{\kappa}} \right) &= 0, \\
\theta'' \left(1 + \frac{16\sigma}{3\kappa^* \varepsilon_3 \kappa} \right) + \left[\frac{A_1 \nu (\rho C)_{nf}}{\varepsilon_3 \kappa} \right] f(\eta) \theta' + \frac{Q_0 h^2}{\varepsilon_3 \kappa} \theta &= 0,
\end{aligned} \tag{4.11}$$

Substitute the value of $(\rho C)_{nf}$ in Eq. (4.11)

$$\begin{aligned}
\theta'' \left(1 + \frac{16\sigma}{3\kappa^* \varepsilon_3 \kappa} \right) + \left[\frac{A_1 \nu}{\varepsilon_3 \kappa} ((1 - \phi) \rho C p + \phi (\rho C)_{cnt}) \right] f(\eta) \theta' + \frac{Q_0 h^2}{\varepsilon_3 \kappa} \theta &= 0, \\
\theta'' \left(1 + \frac{Nr}{\varepsilon_3} \right) + \left[\frac{A_1 \nu (\rho C p)}{\varepsilon_3 \kappa} \left((1 - \phi) + \frac{\phi (\rho C)_{cnt}}{(\rho C)} \right) \right] f(\eta) \theta' + \frac{Q \theta}{\varepsilon_3} &= 0, \\
\theta'' \left(1 + \frac{Nr}{\varepsilon_3} \right) + \left[\frac{A_1 \nu \varepsilon_2 (\rho C p)}{\varepsilon_3 \kappa} \right] f(\eta) \theta' + \frac{Q \theta}{\varepsilon_3}, & \\
\theta'' \left(1 + \frac{Nr}{\varepsilon_3} \right) + \frac{A_1}{\varepsilon_3} \varepsilon_2 P r f(\eta) \theta' + \frac{Q \theta}{\varepsilon_3} &= 0.
\end{aligned} \tag{4.12}$$

Equation (4.12) is the ordinary differential equation in $\theta(\eta)$. Various parameters appearing in Eqs. (4.8), (4.10) and (4.12) are given as

$$\varepsilon_2 = \left[(1 - \phi) + \phi \frac{(\rho C)_{cnt}}{\rho C} \right], \quad \varepsilon_3 = \frac{\kappa_{nf}}{\kappa} = \frac{1 - \phi + 2\phi \left(\frac{\kappa_{cnt}}{\kappa_{cnt} - \kappa} \right) \ln \left(\frac{\kappa_{cnt} + \kappa}{2\kappa} \right)}{1 - \phi + 2\phi \left(\frac{\kappa}{\kappa_{cnt} - \kappa} \right) \ln \left(\frac{\kappa_{cnt} + \kappa}{2\kappa} \right)}. \tag{4.13}$$

$$Pr = \frac{\nu\rho(Cp)}{\kappa}, \quad Nr = \frac{16\sigma T_a^3}{3\kappa^* \kappa}, \quad Q = \frac{Q_0 h^2}{\kappa}. \quad (4.14)$$

The corresponding non-dimensional boundary conditions are
at $\eta = 0$ (corresponding to $y = 0$)

$$f(0) = 0, \quad f'(0) = 1, \quad g(0) = 0, \quad \theta(0) = 0, \quad (4.15)$$

at $\eta = 1$ (corresponding to $y = 1$)

$$f(1) = S, \quad f'(1) = 0, \quad g(1) = 0, \quad \theta'(1) = \frac{-Bi(\theta - 1)}{\varepsilon_3} \quad (4.16)$$

Here S is the suction/injection parameter and $Bi = \frac{ha}{\kappa}$ is the Biot number. The skin friction coefficient and the local Nusselt number are defined as

$$C_f = \frac{\tau_v}{\rho_{nf} U_v^2}, \quad (4.17)$$

$$Nu = \frac{xq_v}{\kappa_{nf}(T_a - T_0)}, \quad (4.18)$$

where $\tau_v = \mu_{nf} \frac{\partial u}{\partial y}$ is the shear stress and $q_v = -\kappa_{nf} \frac{\partial T}{\partial y} + \frac{16\sigma^* T_a^3}{3k^*} \frac{\partial T}{\partial y}$ is the heat flux.

Using similarity transformations from Eq. (4.7), Eq. (4.17) and Eq. (4.18) give

$$C_f^* = \frac{U_v h}{\nu_f} C_f = \frac{f''(\eta)}{\left(\frac{1}{(1-\phi) + \phi \frac{\rho_{cnt}}{\rho}} \right) (1-\phi)^{2.5}}, \quad (4.19)$$

$$Nu_x^* = \frac{h}{x} Nu_x = -\theta'(\eta) \left(1 + \frac{Nr}{\varepsilon_3} \right). \quad (4.20)$$

for $\eta = 0$ and 1.

4.2 Numerical method

The boundary value problem (4.8), (4.10) and (4.12) with boundary condition Eqs. (4.15, 4.16), is solved numerically in this section. Equations (4.8), (4.10) and (4.12) are first converted into a system of first order equations by using following substitutions

$$y_1 = f, \quad y_2 = f', \quad y_3 = f'', \quad y_4 = f''', \quad y_5 = g, \quad y_6 = g', \quad y_7 = \theta, \quad y_8 = \theta'. \quad (4.21)$$

This gives

$$\begin{bmatrix} y_1' \\ y_2' \\ y_3' \\ y_4' \\ y_5' \\ y_6' \\ y_7' \\ y_8' \end{bmatrix} = \begin{bmatrix} y_2 \\ y_3 \\ y_4 \\ \varepsilon_1 A_1 (y_2 y_3 - y_1 y_4) + 2A_2 \varepsilon_1 y_6 + M y_3 \\ y_6 \\ \varepsilon_1 A_1 (y_5 y_2 - y_1 y_6) - 2\varepsilon_1 A_2 y_2 + M y_5 \\ y_8 \\ \frac{1}{(1+Nr/\varepsilon_3)} \left(-\frac{A_1}{\varepsilon_3} \varepsilon_2 Pr y_1 y_8 - \frac{Qy_7}{\varepsilon_3} \right) \end{bmatrix} \quad (4.22)$$

Whereas the relevant boundary conditions from Eq. (4.15-4.16) are

$$\begin{bmatrix} y_1(0) \\ y_2(0) \\ y_5(0) \\ y_7(0) \\ y_1(1) \\ y_2(1) \\ y_5(1) \\ y_7(1) \end{bmatrix} = \begin{bmatrix} 0 \\ 1 \\ 0 \\ 1 \\ S \\ 0 \\ 0 \\ \frac{-Bi(\theta - 1)}{\varepsilon_3} \end{bmatrix} \quad (4.23)$$

Equation (4.22) gives the system of first order ODEs along with boundary conditions Eq. (4.23). This system is solved using *bvp4c* in MATLAB. The following section gives detailed analysis of the solutions.

4.3 Results and discussion

In this section, graphical and tabular results for single and multiple wall C_{NT} are observed with different physical parameters including suction / injection parameter (S), Reynolds number (A_1), rotation parameter (A_2), nanoparticle volume fraction (ϕ), magnetic parameter (M), thermal radiation parameter (Nr) and the heat generation or absorption parameter (Q).

4.3.1 Velocity and temperature

Velocity and temperature graphs are discussed in this subsection

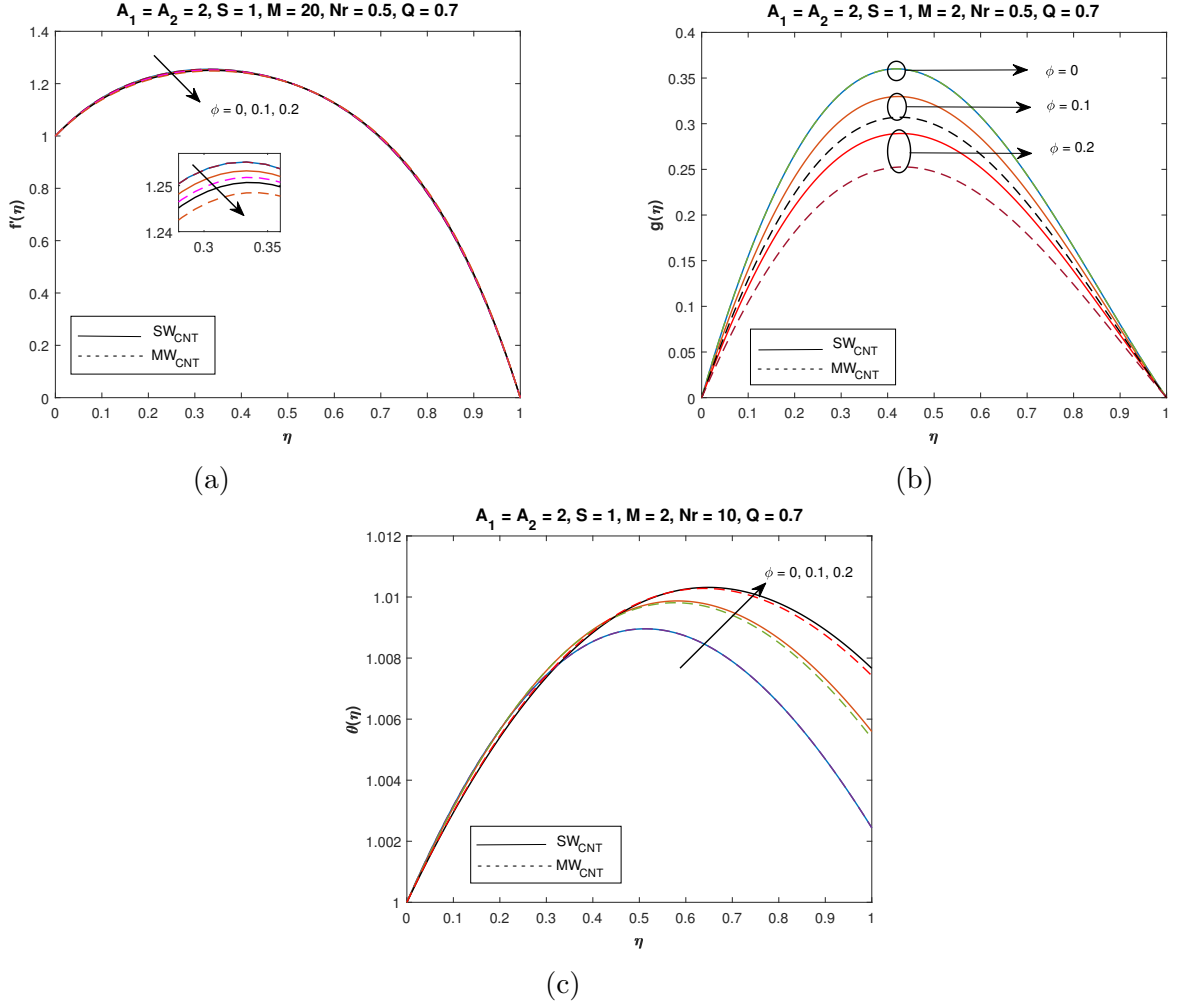


Figure 4.2: Velocity variation in (a-b) and temperature in (c) with respect to η for diverse choices of ϕ with $Bi = 10$.

Figure 4.2(a-b) demonstrate the changes in velocity for diverse choices of ϕ , for SW_{CNT} . Both $f'(\eta)$ and $g(\eta)$ are higher as compared to that for MW_{CNT} . This is opposite to the behavior recorded in the absence of M, Nr and Q in [19]. Figure 4.2(c) shows the fluctuation of θ . For SW_{CNT} , temperature profile is higher than that for MW_{CNT} for a fixed value of ϕ . This is a little different from that shown in [19], as the boundary conditions are different.

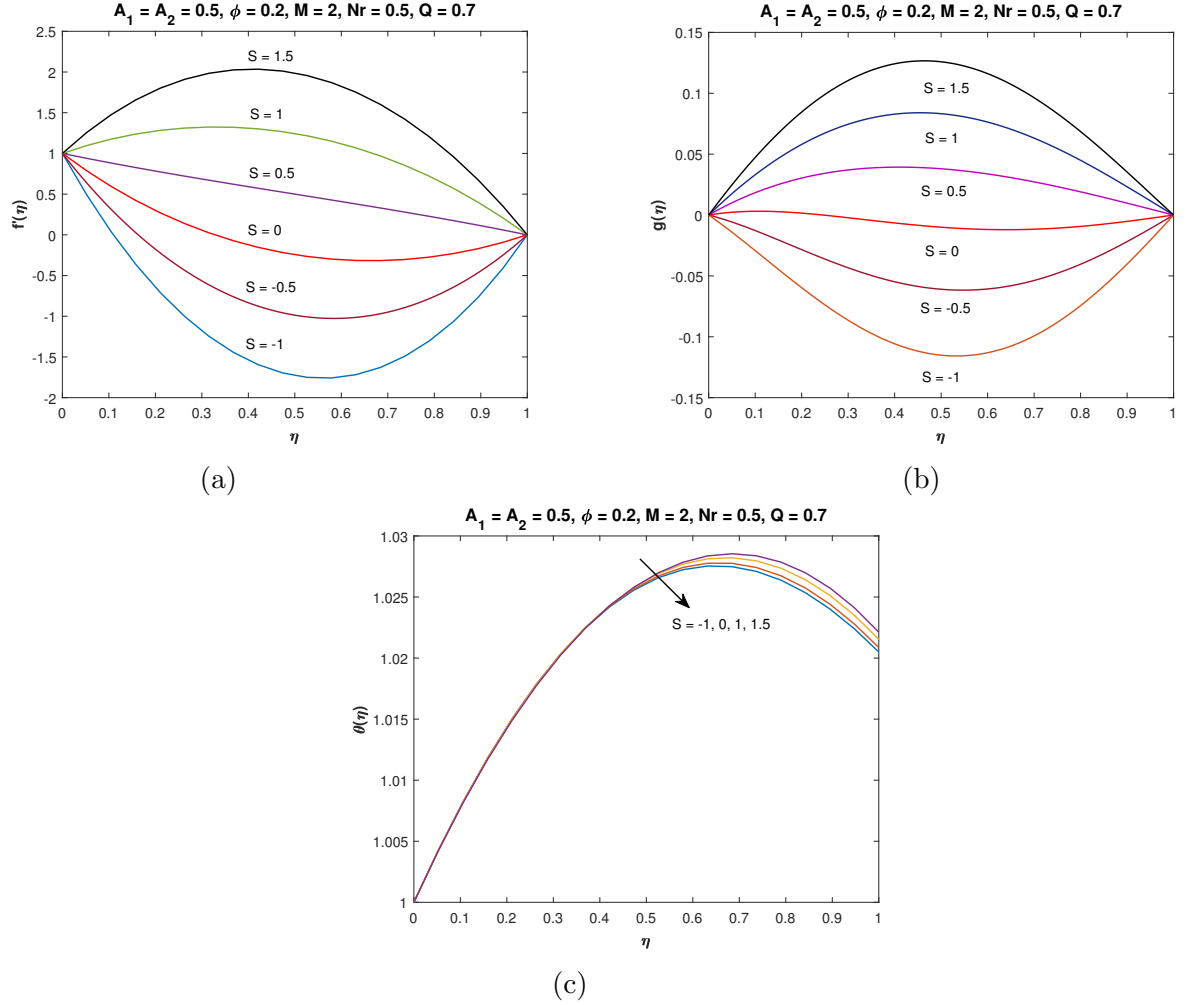


Figure 4.3: Velocity variation in (a-b) and temperature in (c) with respect to η for diverse choices of S with $Bi = 10$.

Figure (4.3)-(4.7) are plotted to show the behaviors of velocity and temperature for varying S , A_1 and A_2 in the case of SW_{CNT} .

Figure 4.3(a-c) depict the changes in velocity and temperature for diverse values of S . In both Figs. 4.3(a-b), the behavior of $f'(\eta)$ and $g(\eta)$ is quite similar to that recorded in [19] which is that the velocity increases with increasing S . In Fig. 4.3(c) temperature decreases with increasing values of S .

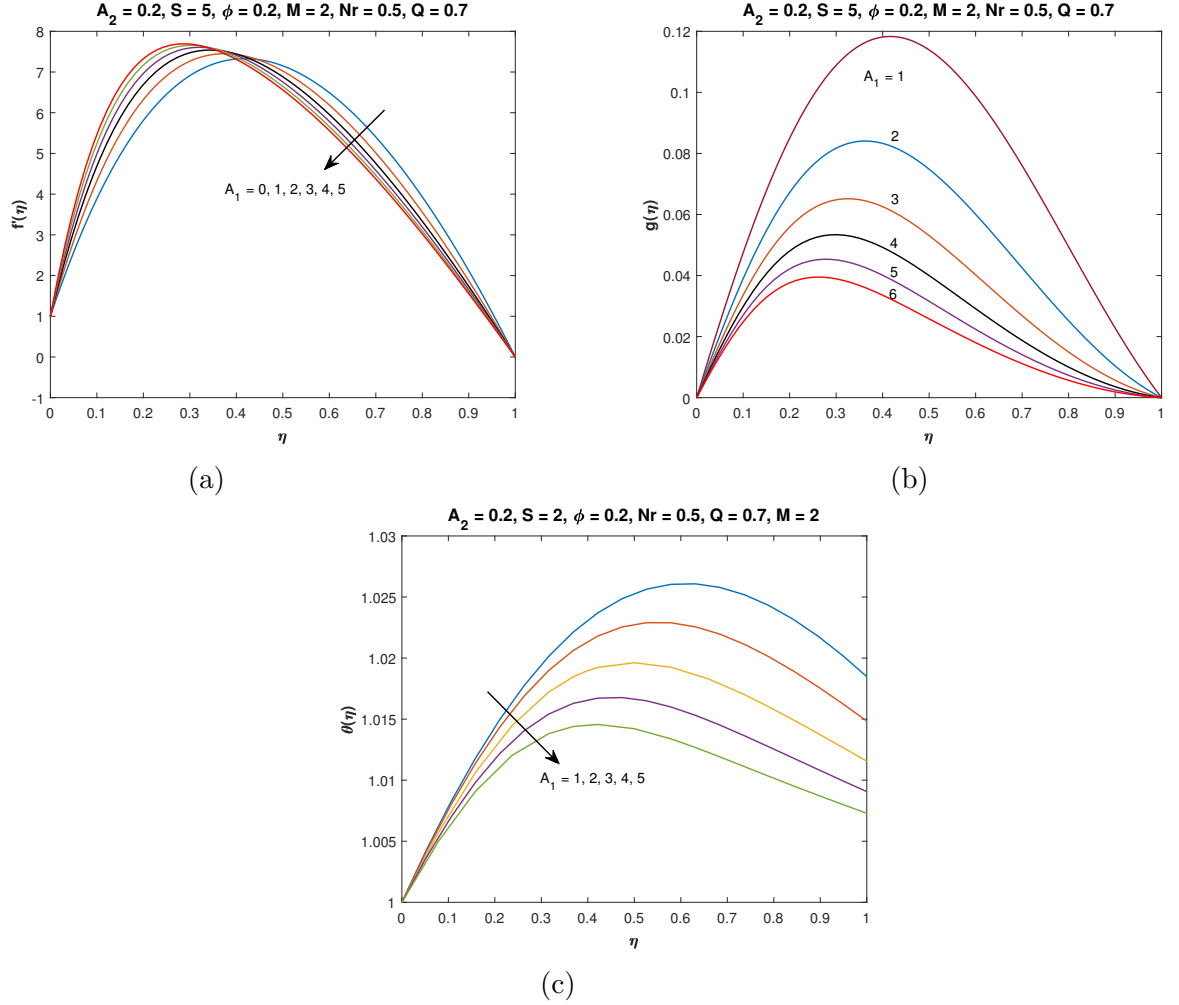


Figure 4.4: Velocity variation in (a-b) and temperature in (c) with respect to η for diverse choices of A_1 with $Bi = 10$.

In Fig. 4.4(a), firstly $f'(\eta)$ is showing an increasing behavior then it decreases at mean position while in Fig. 4.4(b), $g(\eta)$ is decreasing for increasing value of A_1 . This is quite similar to the behavior recorded in [19], in the absence of M, Nr and Q . In Fig. 4.4(c), temperature profile is decreasing with an increase in A_1 .

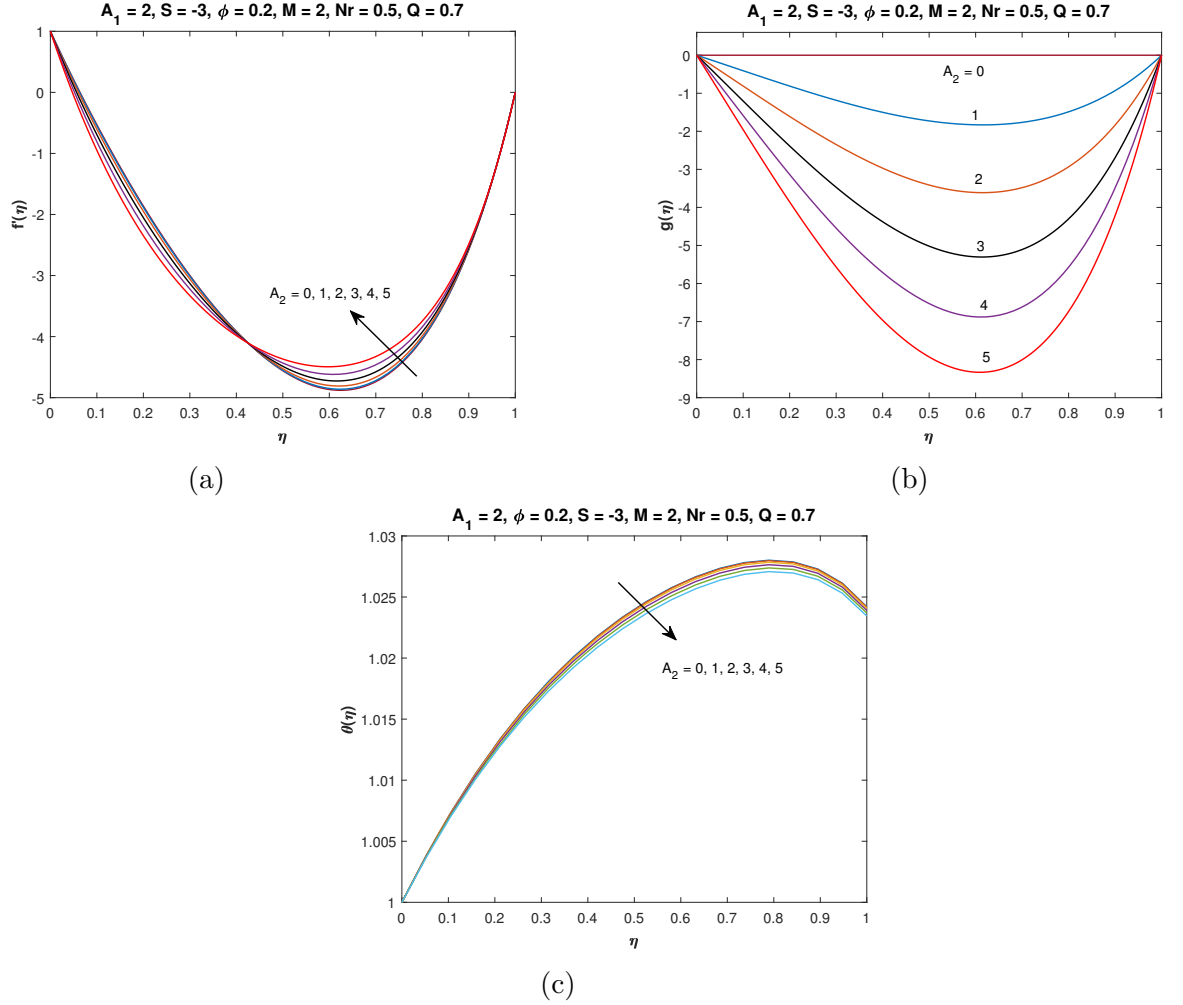


Figure 4.5: Velocity variation in (a-b) and temperature in (c) with respect to η for diverse choices of A_2 with $Bi = 10$.

In Fig. 4.5(a-c) we can observe the fluctuation of velocity and temperature profile for rotation parameter A_2 . In Fig. 4.5(a-b), for different values of A_2 , $f'(\eta)$ and $g(\eta)$ decrease with an increase in η . Variation of $g(\eta)$ is higher at mean position as compared to the boundary. In Fig. 4.5(c), temperature profile shows decreasing behavior with increasing A_2 .

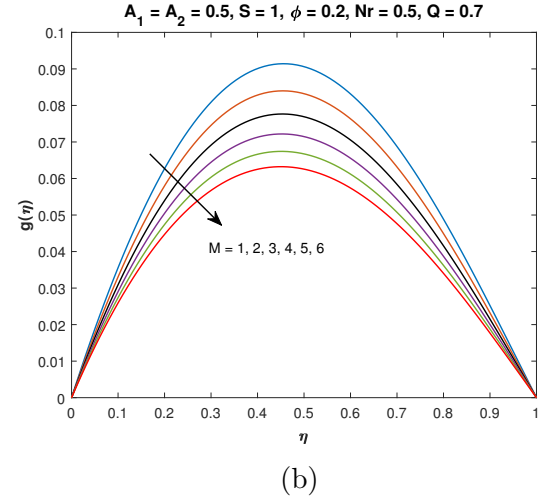
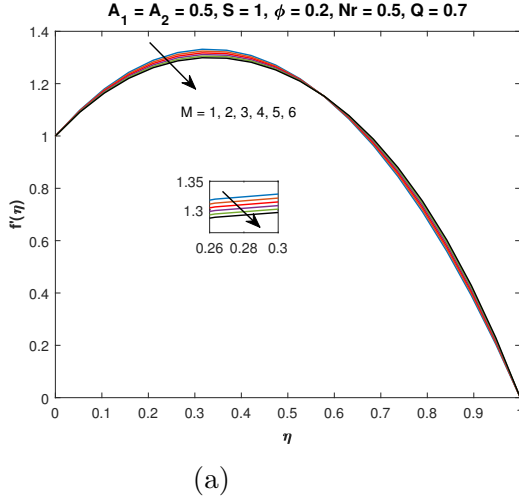


Figure 4.6: Velocity variation with respect to η for diverse choices of M .

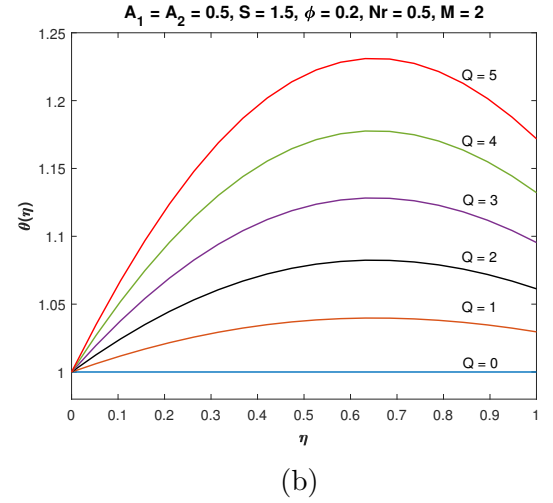
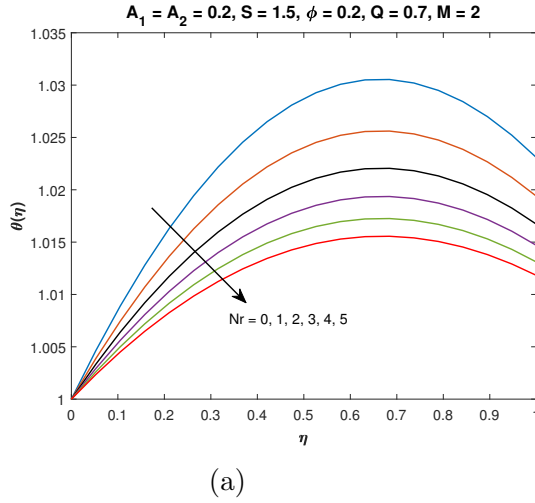


Figure 4.7: Temperature variation for diverse choices of Nr and Q with $Bi = 10$.

Figure 4.6(a-b) illustrates the effect of M on velocity $f'(\eta)$ and $g(\eta)$. The velocity distribution is observed to decrease. The Lorentz force, which opposes fluid motion and decreases fluid freedom of movement, is produced by a magnetic field. Therefore, when magnetic field increases, the retardation force increases as well, and this resistance to the flow is what causes the fluid velocity to decrease.

In Fig. 4.7(a-b), the effect of radiation Nr and heat source Q on temperature of the fluid is represented. As observed in Fig. 4.7(a), an increase in Nr results in decreasing temperature. Figure 4.7(b) displays that the temperature rise as heat source (Q) increases.

4.3.2 Skin friction coefficient (C_f^*) and local Nusselt number (Nu_x^*)

In this section, the comparison between previous results [19] and current results for C_f^* and Nu_x^* at $\eta = 0$ and 1 are shown.

Table 4.1 shows how changes in the S , ϕ and M affect C_f^* at $\eta = 0$. With the rise in M , C_f^* decreases. In case of ϕ , both previous [19] and present results show similar behavior. For $S = 1$, C_f^* increases as ϕ increase but for $S = 0$ and -1 it shows an opposite behavior.

Table 4.2 represents the effect of increasing values of S , ϕ and M on C_f^* at $\eta = 1$. In comparison with Table 4.1, for $S = 0, 1$ behavior of C_f^* is same as M increases but for $S = -1$, value of C_f^* rises. In case of ϕ , behavior of C_f^* is opposite as it was in Table 4.1 for $S = 1$. C_f^* falls with the rising values of ϕ at $S = 1$.

Table 4.3 and 4.4 show the effect of variation of ϕ , S , Nr and Q on Nu_x^* at $\eta = 0$ and $\eta = 1$ respectively. In both cases, Nu_x^* rises with the rising values of Q while it falls with the rising values of Nr and ϕ .

S	ϕ	M	Present skin friction	Results from Hussain et. al [19] ($M = 0$)
-1	0.0	2	-10.2194	-9.750415
	0.1		-11.4843	-10.9595
	0.2		-13.582	-12.965
-1	0.2	1	-13.2767	
		2	-13.582	
		3	-13.8812	
0	0.0	2	-4.30362	-4.04541
	0.1		-4.81925	-4.52952
	0.2		-5.67422	-5.33224
0	0.2	1	-5.50537	
		2	-5.67422	
		3	-5.83904	
1	0.0	2	2.04464	2.1137
	0.1		2.27874	2.35531
	0.2		2.66702	2.75608
1	0.2	1	2.71019	
		2	2.66702	
		3	2.62633	

Table 4.1: Results of skin friction coefficient (Eq. 4.19) for varying choices of ϕ , S and M with $A_1 = A_2 = 0.5$, $Bi = 10$, $Nr = 0.4$, $Q = 0.5$ and $Pr = 6.2$ at $\eta = 0$.

S	ϕ	M	Present skin friction	Results from Hussain et. al [19] ($M = 0$)
-1	0.0	2	8.51706	8.39761
	0.1		9.49932	9.36315
	0.2		11.129	10.9653
-1	0.2	1	11.0465	
		2	11.129	
		3	11.2126	
0	0.0	2	1.91557	1.97626
	0.1		2.15016	2.21844
	0.2		2.53909	2.61996
0	0.2	1	2.5783	
		2	2.53909	
		3	2.50212	
1	0.0	2	-4.14171	-3.89058
	0.1		-4.65604	-4.37324
	0.2		-5.50936	-5.17412
1	0.2	1	-5.34374	
		2	-5.50936	
		3	-5.6715	

Table 4.2: Results of skin friction coefficient (Eq. 4.19) for varying choices of ϕ , S and M with $A_1 = A_2 = 0.5$, $Bi = 10$, $Nr = 0.4$, $Q = 0.5$ and $Pr = 6.2$ at $\eta = 1$.

S	ϕ	Nr	Q	Present local Nusselt number	Results from Hussain et. al [19] ($Nr = Q = Bi = 0$)
-1	0.0	0.5	0.5	0.301895	0.679423
	0.1			0.109816	0.900841
	0.2			0.0649132	0.950317
-1	0.2	0.5	0.5	0.0649132	
		1		0.0648088	
		2		0.0646422	
-1	0.2	0.5	0.5	0.0649132	
			1	0.131662	
			2	0.27106	
0	0.0	0.5	0.5	0.293849	1.161792
	0.1			0.109518	1.049914
	0.2			0.0652628	1.025075
0	0.2	0.5	0.5	0.0652628	
		1		0.0651253	
		2		0.064908	
0	0.2	0.5	0.5	0.0652628	
			1	0.13237	
			2	0.27251	
1	0.0	0.5	0.5	0.277623	1.628918
	0.1			0.108403	1.201072
	0.2			0.0654577	1.101120
1	0.2	0.5	0.5	0.0654577	
		1		0.0653141	
		2		0.0650836	
1	0.2	0.5	0.5	0.0654577	
			1	0.132754	
			2	0.27325	

Table 4.3: Results of local Nusselt number (Eq. 4.20) for varying choices of ϕ , S , Nr and Q with $A_1 = A_2 = 0.5$, $Bi = 10$, $M = 2$ and $Pr = 6.2$ at $\eta = 0$.

S	ϕ	Nr	Q	Present local Nusselt number	Results from Hussain et. al [19] ($Nr = Q = Bi = 0$)
-1	0.0	0.5	0.5	0.319987	2.430418
	0.1			0.0745681	1.352954
	0.2			0.032436	1.167790
-1	0.2	0.5	0.5	0.032436	
		1		0.0323131	
		2		0.0321174	
-1	0.2	0.5	0.5	0.032436	
			1	0.0660433	
			2	0.137031	
0	0.0	0.5	0.5	0.237746	0.898759
	0.1			0.0685953	0.967426
	0.2			0.0315805	0.983472
0	0.2	0.5	0.5	0.0315805	
		1		0.0315236	
		2		0.0314334	
0	0.2	0.5	0.5	0.0315805	
			1	0.0642906	
			2	0.133347	
1	0.0	0.5	0.5	0.167682	0.265542
	0.1			0.0621762	0.674384
	0.2			0.0305971	0.822238
1	0.2	0.5	0.5	0.0305971	
		1		0.0306265	
		2		0.0306707	
1	0.2	0.5	0.5	0.0305971	
			1	0.0622718	
			2	0.129088	

Table 4.4: Results of local Nusselt number (Eq. 4.20) for varying choices of ϕ , S , Nr and Q with $A_1 = A_2 = 0.5$, $Bi = 10$, $M = 2$ and $Pr = 6.2$ at $\eta = 1$.

Chapter 5

Conclusions

In this thesis rotating channel is considered containing MHD nanofluid. In addition to MHD (represented by M), the effects of radiation and heat source are also analyzed. The governing partial differential equations include various parameters such as the injection / suction (S), Reynolds number (A_1), rotation (A_2), radiation (Nr) and heat source (Q). The effects of these parameters are analyzed on velocity, temperature, local nusselt number and the skin friction coefficient. A system of ordinary differential equation is obtained using similarity transformations and the MATLAB built-in function *bvp4c* is used to obtain numerical solutions. These solutions are obtained for representative values of the effective parameters and are illustrated graphically.

The following observations are made:

- As the volume fraction of nanoparticles increases, the velocity and temperature are found to increase.
- Velocity profile decelerates with increasing M .
- As the heat in the system increases, that is with increasing Q , the temperature

of the fluid rises.

- SW_{CNT} have lower skin friction coefficient as compared to MW_{CNT} which indicates that SW_{CNT} produce less resistance to fluid flow.
- As compared to MW_{CNT} , SW_{CNT} show higher heat transfer rate since these bear higher local Nusselt number.

Bibliography

- [1] Masuda, H., Ebata, A., Teramae, K., and Hishinuma, N. (1993). alteration of thermal conductivity and viscosity of liquid by dispersing ultra-fine particles, *Netsu Bussei* 0913-946X, 7(4), pp. 227-233.
- [2] Choi, S.U.S, and Eastman, Jeffrey A. (1995). Enhancing thermal conductivity of fluids with nanoparticles. Argonne National Lab., IL (United States).
- [3] Xie, H., Lee, H., Youn, W., and Choi, M. (2003). Nanofluids containing multi-walled carbon nanotubes and their enhanced thermal conductivities. *Journal of Applied Physics*, 94(8), 4967-4971.
- [4] Hong, H., Wright, B., Wensel, J., Jin, S., Ye, X. R., and Roy, W. (2007). Enhanced thermal conductivity by the magnetic field in heat transfer nanofluids containing carbon nanotube. *Synthetic Metals*, 157(10-12), 437-440.
- [5] Wright, B., Thomas, D., Hong, H., Groven, L., Puszynski, J., Duke, E., Ye, X., and Jin, S. (2007). Magnetic field enhanced thermal conductivity in heat transfer nanofluids containing Ni coated single wall carbon nanotubes. *Applied Physics Letters*, 91(17), pp 1731-116.

- [6] Chamkha, A. J., and Aly, A. M. (2010). MHD free convection flow of a nanofluid past a vertical plate in the presence of heat generation or absorption effects. *Chemical Engineering Communications*, 198(3), 425-441.
- [7] Haq, R. U., Khan, Z. H., and Khan, W. A. (2014). Thermophysical effects of carbon nanotubes on MHD flow over a stretching surface. *Physica E: Low-dimensional Systems and Nanostructures*, 63, 215-222.
- [8] Haq, R. U., Nadeem, S., Khan, Z. H., and Noor, N. F. M. (2015). Convective heat transfer in MHD slip flow over a stretching surface in the presence of carbon nanotubes. *Physica B: condensed matter*, 457, 40-47.
- [9] Motsumi, T. G., and Makinde, O. D. (2012). Effects of thermal radiation and viscous dissipation on boundary layer flow of nanofluids over a permeable moving flat plate. *Physica Scripta*, 86(4), 045003.
- [10] Shehzad, S. A., Hayat, T., Alsaedi, A., and Obid, M. A. (2014). Nonlinear thermal radiation in three-dimensional flow of Jeffrey nanofluid: a model for solar energy. *Applied Mathematics and Computation*, 248, 273-286.
- [11] Hayat, T., Muhammad, T., Alsaedi, A., and Alhuthali, M. S. (2015). Magneto-hydrodynamic three-dimensional flow of viscoelastic nanofluid in the presence of nonlinear thermal radiation. *Journal of Magnetism and Magnetic Materials*, 385, 222-229.
- [12] Sheikholeslami, M., Ganji, D. D., Javed, M. Y., and Ellahi, R. (2015). Effect of thermal radiation on magnetohydrodynamics nanofluid flow and heat transfer by means of two phase model. *Journal of Magnetism and Magnetic Materials*, 374, 36-43.

- [13] Gireesha, B. J., Archana, M., Prasannakumara, B. C., Gorla, R. R., and Makinde, O. D. (2017). MHD three dimensional double diffusive flow of Casson nanofluid with buoyancy forces and nonlinear thermal radiation over a stretching surface. *International Journal of Numerical Methods for Heat and Fluid Flow*.
- [14] Mahanthesh, B., Gireesha, B. J., Gorla, R. S., and Makinde, O. D. (2018). Magneto-hydrodynamic three-dimensional flow of nanofluids with slip and thermal radiation over a nonlinear stretching sheet: a numerical study. *Neural Computing and Applications*, 30(5), 1557-1567.
- [15] Hassan, H., and Harmand, S. (2015). Effect of using nanofluids on the performance of rotating heat pipe. *Applied Mathematical Modelling*, 39(15), 4445-4462.
- [16] Reddy, J. R., Sugunamma, V., Sandeep, N., and Sulochana, C. (2016). Influence of chemical reaction, radiation and rotation on MHD nanofluid flow past a permeable flat plate in porous medium. *Journal of the Nigerian Mathematical Society*, 35(1), 48-65.
- [17] Mohyud-Din, S. T., Hamid, M., Usman, M., Kanwal, A., Zubair, T., Wang, W., and Nazir, A. (2019). Rotating flow of nanofluid due to exponentially stretching surface: an optimal study. *Journal of Algorithms and Computational Technology*, 13, doi:10.1177-1748302619881365.
- [18] Sheikholeslami, M., and Ganji, D. D. (2015). Unsteady nanofluid flow and heat transfer in presence of magnetic field considering thermal radiation. *Journal of the Brazilian Society of Mechanical Sciences and Engineering*, 37(3), 895-902.

- [19] Hussain, S. T., Haq, R. U., Khan, Z. H., and Nadeem, S. (2016). Water driven flow of carbon nanotubes in a rotating channel. *Journal of Molecular Liquids*, 214, 136-144.
- [20] Jawad, M., Shah, Z., Islam, S., Majdoubi, J., Tlili, I., Khan, W., and Khan, I. (2019). Impact of nonlinear thermal radiation and the viscous dissipation effect on the unsteady three-dimensional rotating flow of single-wall carbon nanotubes with aqueous suspensions. *Symmetry*, 11(2), 207.
- [21] White, F. M. (2011), *Fluid mechanics* 7th edition, McGraw-Hill.
- [22] Iijima, S. (1991). Helical microtubules of graphitic carbon. *Nature*, 354(6348), 56-58.
- [23] Haq, R. U., Nadeem, S., Khan, Z. H., and Noor, N. F. M. (2015). Convective heat transfer in MHD slip flow over a stretching surface in the presence of carbon nanotubes. *Physica B: condensed matter*, 457, 40-47.
- [24] Lv, Y. P., Shaheen, N., Ramzan, M., Mursaleen, M., Nisar, K. S., and Malik, M. Y. (2021). Chemical reaction and thermal radiation impact on a nanofluid flow in a rotating channel with Hall current. *Scientific Reports*, 11(1), 1-17.